



A small molecule inhibitor of PCSK9 that antagonizes LDL receptor binding via interaction with a cryptic PCSK9 binding groove

Benny J. Evison^{a,*}, James T. Palmer^b, Gilles Lambert^c, Herbert Treutlein^d, Jun Zeng^e, Brice Nativel^c, Kévin Chemello^c, Qing Zhu^f, Jie Wang^f, Yanfen Teng^f, Wei Tang^f, Yanfeng Xu^f, Anuj Kumar Rathi^g, Sanjay Kumar^g, Alexandra K. Suchowerska^a, Jasneet Parmar^a, Ian Dixon^h, Graham E. Kelly^a, James Bonnar^a

^a Nyrada Inc., 828 Pacific Highway, Gordon, New South Wales 2072, Australia

^b Pharmaceutical Discovery Consultation, 143-145 Flannery Court, Warrandyte, Victoria 3113, Australia

^c Laboratoire Inserm UMR 1188 DÉTROIT, Université de la Réunion Plateforme CYROI, 2 Rue Maxime Rivière, 97490 Sainte Clotilde, France

^d Sanoosa Pty. Ltd., Level 30, 35 Collins St, Melbourne, Victoria 3000, Australia

^e MedChemSoft Solutions, 3 Beech Close, Ferntree Gully, Victoria 3156, Australia

^f ChemPartner, No. 5 Building, 998 Halei Rd, Zhangjiang Hi-Tech Park, Pudong New Area, Shanghai, China

^g Jubilant Chemsys Ltd., B-34, Sector-58, Noida 201301, India

^h Altnia Group, 13 Fuchsia St, Blackburn, Victoria 3130, Australia

ARTICLE INFO

Keywords:

Proprotein convertase (PC) subtilisin kexin type 9 (PCSK9)
Small molecule
Cardiovascular disease
Low density lipoprotein (LDL)
LDL receptor
LDL cholesterol

ABSTRACT

Proprotein convertase (PC) subtilisin kexin type 9 (PCSK9) inhibits the clearance of low density lipoprotein (LDL) cholesterol from plasma by directly interacting with the LDL receptor (LDLR). As the interaction promotes elevated plasma LDL cholesterol levels and a predisposition to cardiovascular disease (CVD), it has attracted much interest as a therapeutic target. While anti-PCSK9 monoclonal antibodies have been successful in the treatment of hypercholesterolemia by decreasing CVD risk, their high cost and a requirement for injection have prohibited widespread use. The advent of an orally bioavailable small molecule inhibitor of the PCSK9-LDLR interaction is an attractive alternative, however efforts have been tempered as the binding interface is unfavourable for binding by small organic molecules. Despite its challenging nature, we report herein the discovery of compound **3f** as a small molecule inhibitor of PCSK9. The kinase inhibitor nilotinib emerged from a computational screen that was applied to identify compounds that may bind to a cryptic groove within PCSK9 and proximal to the LDLR-binding interface. A subsequent *in vitro* PCSK9-LDLR binding assay established that nilotinib was a bona fide but modest inhibitor of the interaction ($IC_{50} = 9.8 \mu M$). Through multiple rounds of medicinal chemistry, **3f** emerged as a lead-like molecule by demonstrating disruption of the PCSK9-LDLR interaction at nanomolar levels *in vitro* ($IC_{50} = 537 \text{ nM}$) with no inhibitory activity ($IC_{50} > 10 \mu M$) against a small panel of kinases. Compound **3f** restored LDL uptake by liver cells at sub-micromolar levels and demonstrated excellent bioavailability when delivered subcutaneously in mice. Most significantly, compound **3f** lowered total cholesterol levels in the plasma of wild-type mice, thereby providing proof-of-concept that the notion of a small molecule inhibitor against PCSK9 is therapeutically viable.

* Corresponding author.

E-mail address: benny.evison@nyrada.com (B.J. Evison).

<https://doi.org/10.1016/j.bmc.2020.115344>

Received 23 August 2019; Received in revised form 17 January 2020; Accepted 23 January 2020

Available online 31 January 2020

0968-0896/ © 2020 The Author(s). Published by Elsevier Ltd. This is an open access article under the CC BY-NC-ND license (<http://creativecommons.org/licenses/by-nc-nd/4.0/>).

1. Introduction

Proprotein convertase (PC)¹ subtilisin kexin type 9 (PCSK9) is a member of the PC family of proteins, a group of nine serine proteases that have been characterised in humans and other organisms.¹ The protein is first synthesised as a zymogen (Fig. 1A) in the ER of cells mainly in the liver, kidney and intestines.^{2,3} Following translation, the signal peptide (residues 1–30) is first excised from the PCSK9 polypeptide which then undergoes an autocatalytic event that cleaves the bond between Gln 152 and Ser 153 of the protein (Fig. 1A and Supplementary Fig. S1).^{1,3–5} It is this second cleavage event that yields the mature protein which consists of a prodomain (residues 30–152), catalytic domain (residues 153–451) and a C-terminal domain (residues 452–692, Fig. 1 and Supplementary Fig. S1).^{2–4} Despite its covalent excision from the protein, the prodomain remains non-covalently associated with the catalytic domain through hydrogen bonding (Fig. 1B).² Importantly, this interaction renders the mature protein catalytically inactive as the prodomain sterically occludes substrate entry into the enzyme's active site (Fig. 1B).^{2,3,5} Once cleavage is achieved, PCSK9 is directed through the *trans*-Golgi network to the plasma membrane and secreted into the extracellular space.¹

The functional characterisation of PCSK9 emerged from studies involving its original identification. Abifadel *et al.*⁶ reported that humans carrying gain-of-function mutations within the PCSK9 gene were susceptible to increased levels of low-density lipoprotein cholesterol (LDL-c), a predominant feature of cardiovascular disease (CVD). Soon after, it was demonstrated that the converse was also true; individuals bearing loss-of function mutations in the gene encoding PCSK9 typically displayed reduced plasma LDL-c⁷ and experienced fewer CVD events.⁸ Functional studies in the ensuing years established that PCSK9 was a key regulator of LDL metabolism; following its secretion from liver cells into blood plasma⁹, PCSK9 engages the EGF(A) domain of the LDL receptor (LDLR) expressed at the plasma membrane of liver cells.^{1,10,11} The LDLR-PCSK9 interaction then promotes the internalisation and subsequent degradation of LDLR within the hepatocyte lysosomal compartment, thereby reducing hepatocyte LDLR expression at the cell surface.^{2,10,11} The pathway culminates in a net decrease in the clearance of plasma LDL-c by hepatocytes and elevated LDL-c plasma levels.¹⁰ It was quickly realised that disruption of the LDLR-PCSK9 interaction may be harnessed to therapeutically lower plasma LDL-c and the risk of CVD in humans.

The EGF(A)-interacting site of PCSK9 is a solvent-exposed area of

~530 Å² that is largely flat, featureless and devoid of binding pockets (Fig. 1B), making it unfavourable for binding by small organic molecules.^{10–13} Characteristics such as these are more conducive to targeting via antibodies raised against the protein. Indeed, much effort led to the development of anti-PCSK9 monoclonal antibodies that have demonstrated excellent LDL-c lowering activity in human clinical trials when used in combination with statin-based therapies.^{9,14,15} Most importantly, the therapies significantly reduced the risk of CVD^{9,15}, thereby validating the inhibition of PCSK9 as therapeutically relevant.

Despite their clinical success, the application of monoclonal antibodies as lipid-lowering therapies has its disadvantages. Monoclonal antibodies are typically very expensive to purchase and must be administered via injection on a regular basis.^{9,16,17} Moreover, there are issues with shelf-life and their propensity to elicit immunogenic responses.¹⁷ Various alternative strategies have been devised to address at least some of these limitations. The application of small interfering RNAs¹⁸, locked antisense nucleic acids¹⁹ and CRISPR-Cas9-based technologies^{20,21} to downregulate PCSK9 protein expression are at various stages of development, yet these have inherent disadvantages of their own.

An attractive alternative would be the advent of an orally bioavailable small molecule inhibitor of PCSK9. A small molecular weight agent directed against PCSK9 is highly sought after as a therapy for CVD, especially given the low cost and ease of administration associated with such agents.¹⁷ A handful of small molecule programs directed at the inhibition of PCSK9 have been described. Pfizer has reported the identification of a small molecule PCSK9 anti-secretagogue^{16,22,23}, however this program has not progressed into the clinic. Several groups including Genentech have identified small peptides that bind directly to PCSK9 and disrupt the protein's interaction with LDLR.^{10–12} Others including Portola, Shifa and Cadila Healthcare have not reported any small molecules beyond the discovery stage²⁴ and very few have been reported in the primary literature in detail.^{17,25} Despite the challenging nature of targeting PCSK9 with small molecular weight agents, we report herein the identification of a small molecule inhibitor of PCSK9 that disrupts the PCSK9-LDLR interaction at nanomolar levels *in vitro*, restores LDL uptake by liver cells cultured in the presence of PCSK9 and lowers total cholesterol levels in the plasma of wild-type mice.

2. Materials and methods

2.1. Materials

DMSO, DMAC, Ficoll Paque Plus, BSA and ATP were from Sigma (St Louis, MO, USA and Saint Quentin-Fallavier, France). Nilotinib was purchased from TRC Inc (Toronto, Canada) while AMB-657286 was from Ambinter (Greenpharma SAS, Orleans, France). Alirocumab was from Sanofi (Chilly-Mazarin, France) while evolocumab was from Amgen (Boulogne-Billancourt, France). Solutol HS15 was from BASF (Ludwigshafen, Germany) and isoflurane was purchased from Hebei Yipin Pharmaceutical Co. LTD (Guangdon, China). The tyrosine kinases Src, PDGFR-β and Abl were purchased from Carma Biosciences (Kobe, Japan) while cKit was obtained from Millipore (Billerica, MA, USA). Peptides FAM-P2, FAM-P4 and FAM-P22 were acquired from GL Biochem (Shanghai, China) while Coating reagent #3 was from Perkin Elmer (Waltham, MA, USA). K2EDTA tubes were from Adamas-Beta (Shanghai, China) while CircuLex PCSK9-LDLR *in vitro* binding assay kits, CircuLex PCSK9 ELISA kits and mutant PCSK9-D374Y were from CycLex (Nagano, Japan). Allophycocyanin-conjugated antibody against the human LDLR and an IgG1 isotype control were from R&D Systems (Lille, France). Cholesterol and Triglyceride FS colorimetric assay kits were purchased from DiaSys, Thermo-Fisher Scientific (Illkirch, France). Bodipy FL LDL was acquired from Invitrogen (Invitrogen, Paisley, UK). RPMI and FBS were from Life Technologies (Saint Aubin, France).

¹ 4A MS, molecular sieve 4A; Abl, Abelson tyrosine kinase; AMB657286, 4-[4-(benzyloxy)-3-methylbenzoyl]-3-hydroxy-1-[3-(4-morpholinyl)propyl]-5-(4-pyridinyl)-1,5-dihydro-2H-pyrrol-2-one; BBFO, broad band fluorine observe; BBO, broad band observe; Bcr-Abl, breakpoint cluster region Abelson tyrosine kinase fusion protein; BOC, *tert*-butyloxycarbonyl; Bodipy FL LDL, boron-dipyrromethene labelled low density lipoprotein (LDL) from human plasma; BPO, benzoyl peroxide; c-Kit, tyrosine protein kinase Kit; CRISPR, clustered regularly interspaced short palindromic repeats; CVD, cardiovascular disease; CYP450, cytochrome P450; DCM, dichloromethane; DIBAL-H, diisobutylaluminium hydride; DIEA or DIPEA, *N,N*-diisopropylethylamine; DMA or DMAC, dimethylacetamide; DMEDA, 1,2-dimethylethylenediamine; DMF, dimethylformamide; DMSO, dimethyl sulfoxide; EGF(A), epidermal growth factor (A); ELISA, Enzyme-linked immunosorbent assay; ER, endoplasmic reticulum; ESI, electrospray ionisation; FAM, fluorescein amidite; HATU, O-(7-azabenzotriazol-1-yl)-*N,N,N',N'*-tetramethyluronium hexafluorophosphate; HepG2, human hepatocarcinoma cell line; IV, intravenous; LAH; Lithium aluminium hydride; LDL, low density lipoprotein; LDL-c, low density lipoprotein (LDL) cholesterol; LDLR, low density lipoprotein (LDL) receptor; NBS, *N*-bromosuccinimide; NMP, *N*-methyl-2-pyrrolidone; PC, proprotein convertase; PCSK9, Proprotein convertase (PC) subtilisin kexin type 9; PO, oral; PDGFRβ; platelet derived growth factor receptor β; SAR, structure activity relationship; SC, subcutaneously; Src, Src tyrosine kinase; Solutol HS15, poly-oxethylene esters of 12-hydroxystearic acid; TFA, trifluoroacetic acid; THF, tetrahydrofuran; TOTP, Tri-*o*-tolyl phosphate

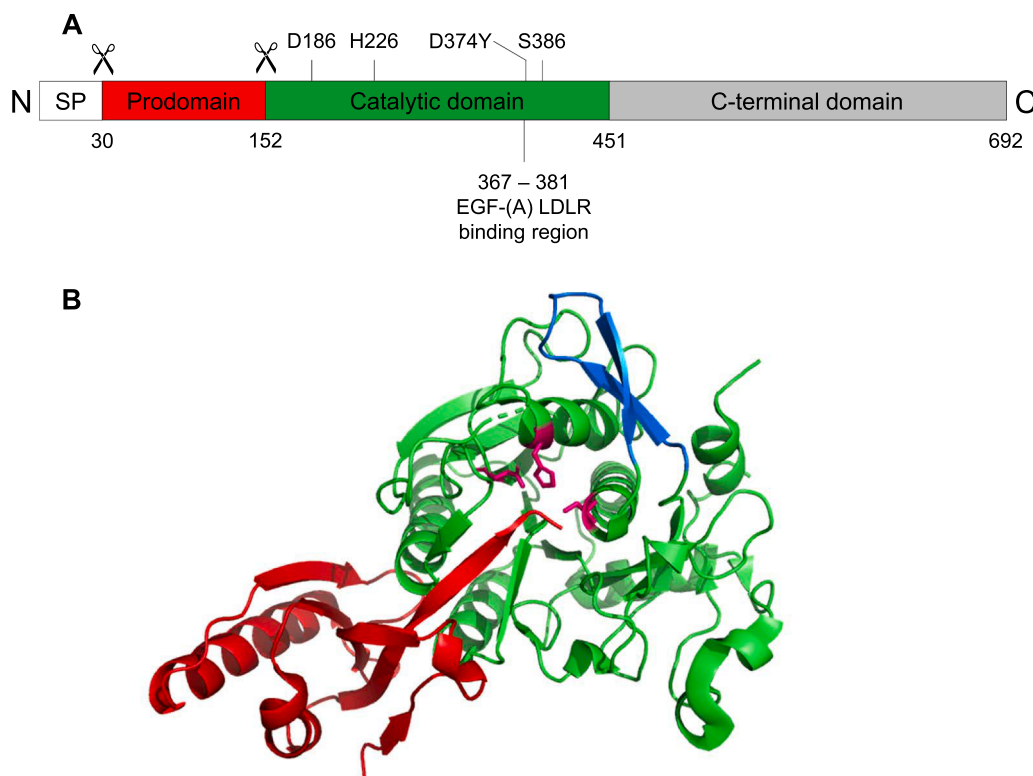


Fig. 1. (A) The domain structure of human PCSK9 in its zymogen form. The numbering throughout indicates the position of significant amino acid residues including D186, H226 and S386, which form the catalytic triad of PCSK9. D374Y indicates an amino acid substitution that has been characterised as a gain-of-function mutation. SP denotes signal peptide. Proteolytic cleavage sites are denoted by a scissors icon. Adapted from^{1 and 3}. (B) A three-dimensional cartoon representation of the X-ray crystal structure of human PCSK9 lacking its C-terminal domain. The prodomain is coloured in red, the catalytic domain in green and the catalytic residues D186, H226 and S386 in pink. The region of PCSK9 that directly interacts with the EGF-(A) domain of LDLR is shown in blue. Adapted from PDB file code 4NMX.¹⁰

2.2. Methods

2.2.1. In silico screening

More than 1100 FDA-approved drugs from the database BindingDB²⁶ were subjected to a virtual screen by computationally docking each compound into PCSK9 using the software package QUBit.²⁷ The structure of PCSK9 described by Lo Surdo *et al.*²⁸ and represented in PDB²⁹ file code 3P5C was adopted for screening, however the prodomain (Fig. 1B) was omitted. The binding site of interest within PCSK9 was defined by amino acid residues His 226, Leu 230, Leu 253, Thr 264, Leu 286, Leu 289, Ala 290, Leu 297, Asn 317 and Ser 386 (Supplementary Fig. S1). Virtual screening was conducted as described previously.³⁰

2.2.2. Chemical synthesis

Small scale synthesis of compounds **1a–1h**, **2a–2f** and **3a–3f** was performed at ChemPartner (Shanghai, China) as detailed in the Supplementary Information. A larger preparation of **3f** (batch J996) was synthesised at Jubilant Chemsys (Noida, India) and is reported herein. A summary of the reaction scheme is provided in Fig. 2. All compounds were synthesized at a purity of greater than 95%. Data displaying the characterization of all compounds by ¹H NMR and LCMS is provided in the Supplementary Information.

2.2.2.1. General methods. The yields reported herein refer to purified products (unless specified). Analytical TLC was performed on Merck silica gel 60 F₂₅₄ aluminium-backed plates. Compounds were visualised by UV light and/or stained with I₂, ninhydrin or potassium permanganate solution followed by heating. Flash column chromatography was performed on silica gel. ¹H NMR spectra were recorded on a Bruker 400 MHz, Avance II spectrometer with a 5 mm DUL (Dual) 13C probe and Bruker 400 MHz, Avance III HD spectrometer with BBFO (Broad Band Fluorine Observe) probe. Chemical shifts (δ) are expressed in parts per million (ppm) with reference to the deuterated solvent peak in which the sample was

prepared. Splitting patterns are designated as s (singlet), d (doublet), t (triplet), q (quartet), m (multiplet) and br s (broad singlet). The following solvents, reagents or scientific terminology may be referred to by their abbreviations.

2.2.2.2. Synthesis of (S)-N-(3-((3-aminopiperidin-1-yl)methyl)-5-(4-methyl-1H-imidazol-1-yl)phenyl)-4-methyl-3-phenoxybenzamide

(3f). DIBAL-H (1 M in toluene, 346 mL, 346 mmol) was slowly added to a solution of **44** (30 g, 115 mmol) in THF (600 mL) at -78°C and the temperature of the mixture slowly warmed to -50°C throughout the addition. The mixture was then allowed to come to room temperature and further stirred for 3 h. The reaction was subsequently cooled to -20°C , quenched with saturated ammonium chloride solution (1000 mL) and then stirred for 30 min. A white suspension was filtered through a celite pad and washed with EtOAc (2×1000 mL). The organic layer was separated and washed with water (500 mL), dried over anhydrous sodium sulphate and concentrated under vacuo to give **65** (26 g, 97.1%) as a brown solid. ¹H NMR (400 MHz; DMSO-*d*₆): δ 8.24 (s, 1H), 8.17 (s, 1H), 7.96 (s, 1H), 5.64 (t, 1H), 4.62 (d, 2H). LCMS: *m/z* 230.87 (M-H)⁻, 73.2%.

To a solution of **65** (26 g, 112 mmol) in DMF (364 mL), **1** (32.2 g, 392 mmol), L-proline (6.45 g, 56 mmol), CuI (17.07 g, 89.6 mmol) and K₂CO₃ (38.7 g, 280 mmol) were sequentially added at room temperature under N₂. The reaction mixture was then heated at 130°C for 18 h. Following the consumption of starting material, the reaction mixture was cooled to room temperature and water (1000 mL) was added to it. The reaction mass was then filtered through a celite pad and then washed with EtOAc (2×500 mL). The filtrate was subsequently extracted with ethyl acetate (2×500 mL), washed with brine (2×500 mL), dried (Na₂SO₄) and concentrated under vacuo to give crude residue. The residue was triturated by EtOAc (3×250 mL) to give **66** (12 g, 45.9%) as a light brown solid. ¹H NMR (400 MHz; DMSO-*d*₆): δ 8.34–8.30 (m, 2H), 8.12 (s, 1H), 8.01 (s, 1H), 7.64 (bs, 1H), 5.64 (t, 1H), 4.67 (d, 2H), 2.17 (s, 3H). LCMS: *m/z* 234.1 (M + H)⁺, 93.9%.

Et₃N (28 mL, 205 mmol) was subsequently added to a solution of **66**

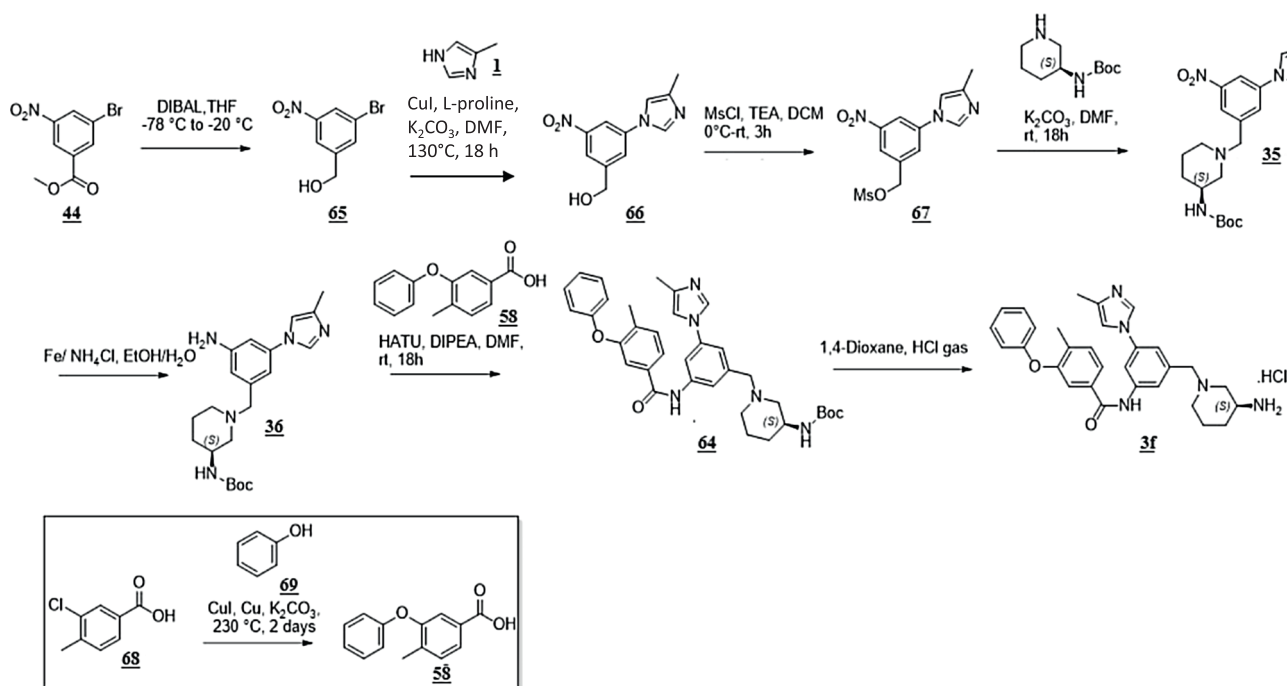


Fig. 2. The synthetic route used to generate compound **3f**.

(12 g, 51.4 mmol) in DCM (240 mL) and stirred at room temperature for 15 min. Methane sulfonylchloride (7.95 mL, 102 mmol) was then slowly added at 0 °C and the reaction stirred at room temperature for a further 3 h. The progress of the reaction was monitored by TLC and after consumption of starting material, the reaction mixture was quenched with water (500 mL) and extracted with DCM (2 × 250 mL). The combined organic layer was washed with brine (200 mL), dried anhydrous with sodium sulphate and concentrated under vacuo to give **67** (11 g, crude, 93.6%) as a brown gummy liquid. The crude preparation was used in the next step without further purification.

K_2CO_3 (12.2 g, 88.3 mmol) was added to a solution of *tert*-butyl (*S*)-piperidin-3-ylcarbamate (7.07 g, 35.3 mmol) in dry DMF (68.2 mL) and stirred for 10 min prior to the addition of **67** (11 g, crude). The resulting mixture was stirred at room temperature for 18 h, and the progress of reaction was monitored by TLC which showed consumption of starting material. The reaction mixture was then diluted with water (500 mL) and extracted with EtOAc (2 × 500 mL). The combined organic layer was washed with brine solution (200 mL), dried with sodium sulphate and concentrated under vacuo to give a crude residue. The residue was purified by combi flash using 3% MeOH/DCM to give **35** (11 g, 58.6%) as a yellow solid. 1H NMR (400 MHz; $DMSO-d_6$): δ 8.40–8.30 (m, 2H), 8.05 (s, 1H), 8.01 (s, 1H), 7.64 (s, 1H), 6.74 (d, $J = 7.2$ Hz, 1H), 3.70–3.60 (m, 2H), 3.52–3.40 (m, 1H), 2.80–2.70 (m, 1H), 2.71–2.60 (m, 1H), 2.17 (s, 3H), 2.02–1.82 (m, 2H), 1.72–1.60 (m, 2H), 1.50–1.40 (m, 2H), 1.38 (s, 9H). LCMS: m/z 416.24 ($M + H$)⁺, 86.5%.

To a stirred solution of **35** (11 g, 26.4 mmol) in EtOH:H₂O (6:1, 385 mL), ammonium chloride (8.48 g, 158.8 mmol) and Fe-powder (13.29 g, 238 mmol) were added. The reaction mixture was stirred at 70 °C for 3 h and progress of reaction mixture was monitored by TLC which showed consumption of starting material. The reaction mixture was then cooled to room temperature and filtered through a celite pad followed by a wash with EtOH (250 mL). The filtrate was concentrated to dryness and then diluted with DCM (1000 mL) and water (500 mL). The collected organic layer was dried over anhydrous sodium sulphate and concentrated under vacuo to give **36** (10 g, 98.03%) as a yellow solid. 1H NMR (400 MHz; $DMSO-d_6$): δ 7.89 (s, 1H), 7.22 (s, 1H), 6.62–6.50 (m, 2H), 6.47 (s, 1H), 5.33 (bs, 2H), 3.52–3.36 (m, 3H), 2.82–2.72 (m, 1H), 2.70–2.60 (m, 1H), 2.13 (s, 3H), 1.90–1.82 (m, 1H),

1.72–1.60 (m, 3H), 1.20–1.40 (m, 2H), 1.35 (s, 9H). LCMS: m/z 386.25 ($M + H$)⁺, 85.4%.

To a solution of **68** (15.0 g, 87.9 mmol), **69** (77.3 mL, 87.9 mmol), Cu-powder (2.79 g, 43.9 mmol), CuI (8.37 g, 43.9 mmol) and K_2CO_3 (24.3 g, 175 mmol) were mixed in a steel vessel and stirred for 2 days at 230 °C. Progress of the reaction mixture was monitored by TLC and LCMS. The resulting mixture was diluted with EtOAc (250 mL), 1 N NaOH (500 mL) and stirred for 1 h at room temperature. The aqueous layer was extracted with EtOAc (3 × 250 mL) and then acidified with 1 N HCl solution (pH 2) and extracted with EtOAc (3 × 250 mL). The organic layer was washed with brine solution (1 × 250 mL), dried with anhydrous sodium sulphate and then concentrated under vacuo to give **58** (8.0 g, 39.8%) as a white solid. 1H NMR (400 MHz; $DMSO-d_6$): 12.96 (s, 1H), 7.64 (d, 1H), 7.46–7.38 (m, 3H), 7.30 (s, 1H), 7.15 (t, 1H), 6.97 (d, 2H), 2.27 (s, 3H).

HATU (13.7 g, 36.1 mmol) and DIPEA (16.78 mL, 96.3 mmol) were sequentially added to a solution of **58** (5.5 g, 24 mmol) in dry DMF (110 mL) at room temperature. After 15 min stirring at this temperature, **36** (10 g, 26.0 mmol) was added. The reaction mixture was stirred at room temperature for 18 h and progress of reaction mixture was monitored by TLC which showed consumption of starting material. The resulting mixture was diluted with water (300 mL) and then extracted with ethyl acetate (2 × 500 mL). The organic layer was washed with brine solution (8 × 250 mL), dried over anhydrous sodium sulphate and concentrated under vacuo to give crude residue. The residue was purified by combi flash using 2% MeOH/DCM to give **64** (8.7 g, 60.6%) as a brown solid. LCMS: m/z 596.39 ($M + H$)⁺, 98.06%.

To a solution of **64** (8.7 g, 14.60 mmol) in 1,4-dioxane (435 mL), HCl (g) was purged at 0–25 °C for 2 h. The reaction mixture was concentrated under vacuo to give crude material which was a slurry in EtOAc (2 × 250 mL) and filtered. The solid material was dissolved in water (150 mL), acetonitrile (50 mL) and lyophilized to give **3f**. HCl (8.2 g, 93.07%). 1H NMR (400 MHz; $DMSO-d_6$ with D₂O): δ 9.35 (s, 1H), 8.08 (s, 1H), 7.94 (s, 1H), 7.82 (s, 1H), 7.74–7.72 (d, 1H), 7.64 (s, 1H), 7.51–7.49 (d, 1H), 7.42–7.36 (m, 2H), 7.14–7.10 (t, 1H), 6.94–6.92 (d, 2H), 4.32–4.30 (d, 2H), 3.43 (bs, 2H), 3.27 (bs, 1H), 2.86 (bs, 2H), 2.32 (s, 3H), 2.25 (s, 3H), 1.98–1.90 (m, 2H), 1.76–1.73 (m, 1H), 1.51 (m, 1H). LCMS: m/z 495.26 ($M + H$)⁺, 98.47%.

2.2.3. *In vitro* PCSK9-LDLR binding assay

Compounds were screened for their inhibitory activity against the PCSK9-LDLR interaction using a CircuLex PCSK9-LDLR *in vitro* binding assay kit according to the manufacturer's instructions. Briefly, stock solutions of test compounds were prepared as 10 mM stocks in DMSO and then serially diluted in 1 × reaction buffer by dispensing each dilution into the wells of a microplate pre-coated with the LDLR-EGF-AB domain. Recombinant human His-tagged PCSK9 (7 ng) was subsequently added to the reaction mix (100 μL reaction volume) and then incubated at room temperature while shaking at 300 rpm for 3 h before washing thoroughly (4 ×) with wash buffer. A biotinylated anti-His tag monoclonal antibody (1 × 100 μL of conjugate dilution buffer) was added to each well and the microplate incubated for a further 1 h at room temperature while shaking at 300 rpm. After washing each well again 4 × with wash buffer, HRP-conjugated streptavidin (100 μL) was added and the microplate incubated at room temperature for 20 min, shaking at 300 rpm. The samples were subjected to a final thorough wash (4 ×) with wash buffer before the addition of substrate reagent (100 μL) to each well. The microplate was then shaken at 300 rpm for a further 15 min at room temperature and the reaction terminated by the addition of stop solution (100 μL). The absorbance of each sample was measured at 450 nm and 540 nm using an EnSpire Multimode Plate Reader (Perkin Elmer, Waltham, MA, USA). The percent inhibition of binding (y-axis) was plotted as a function of compound concentration (x-axis) and the IC₅₀ determined for each compound.

2.2.4. *In vitro* kinase assays

All compounds were initially prepared as 10 mM stocks in DMSO and subsequently diluted in DMSO to 50 × their final concentrations. Ten μL of each DMSO dilution was transferred to a well in a fresh 96-well cluster plate containing 90 μL 1 × Kinase buffer (50 mM HEPES pH 7.5, 10 mM MgCl₂, 2 mM DTT and 0.01% Brij-35) and then mixed for 10 min. Five μL of each compound dilution was subsequently added to a 384-well plate in duplicate. Ten μL of enzyme solution containing either Src, cKit, PDGFR-β or Abl (final concentrations 0.6, 6, 10 or 0.9 nM, respectively) in 1 × Kinase buffer was then added to each well and the mix incubated at room temperature for 10 min. To initiate each reaction, 10 μL of peptide solution containing FAM-labelled peptide (final concentrations 3 μM FAM-P2 for Abl, 3 μM FAM-P22 for cKit and PDGFR-β or 3 μM FAM-P4 for Src) and ATP (final concentrations 36, 6, 40 and 12 μM for Src, cKit, PDGFR-β or Abl, respectively) in 1 × Kinase buffer was added to each well. All reactions were incubated at 28 °C for 1 h and then terminated by the addition of 25 μL stop buffer (100 mM HEPES pH 7.5, 50 mM EDTA, 0.2% Coating Reagent #3 and 0.015% Brij-35). All samples were then subjected to analysis using an EZ Reader II (Caliper Life Sciences, Waltham, MA, USA) (downstream voltages –500 V, upstream voltages –2250 V, base pressure –0.5 PSI, screen pressure –1.2 PSI) to read conversion values. Conversion values were transformed into % inhibition of kinase activity using the formula:

$$\% \text{ Inhibition} = [(M_A - X)/(M_A - M_I)] \times 100\%$$

where M_A = conversion value of DMSO only controls, M_I = conversion value of no enzyme controls and X = conversion value at any given compound dose. IC₅₀ values were then calculated by plotting dose–response curves using the XLfit application in Excel software.

2.2.5. Biolayer interferometry binding analyses

The interaction of evolocumab and compound **3f** with recombinant human PCSK9 was analysed by biolayer interferometry using an Octet® RED96 system (ForteBio, Pall Life Sciences, Menlo Park, CA, USA). Evolocumab (1.25 μg/mL) was initially loaded onto a Dip and Read Anti-hIgG Fc Capture (AHC) biosensor in 1 × kinetic buffer. Recombinant human PCSK9 (1.56–50 nM) was subsequently allowed to associate with captured evolocumab in 1 × assay buffer (1 × kinetic buffer, 0.1% glycerol) for 5 min and then permitted to dissociate for a further 10 min. For analyses involving compound **3f** and recombinant

human PCSK9, the protein was initially biotinylated using an EZ-link NHS-PEG4-biotin reagent (Thermo-Fisher Scientific) and then desalted using a Zeba spin desalting column (Thermo-Fisher Scientific). Biotinylated PCSK9 (27 μg/mL) was subsequently loaded onto a Dip and Read Super Streptavidin (SSA) biosensor followed by a blocking step with biocytin. Compound **3f** (0.2–25.6 μM) was permitted to associate with captured PCSK9 for 2 min and then allowed to dissociate for a further 10 min.

2.2.6. LDL HepG2 cell-uptake assay

Human liver HepG2 cells (ChemPartner, Shanghai, China) were seeded in 96-well cluster plates at 2 × 10⁵ cells/mL (100 μL) and allowed to attach overnight. The gain-of-function PCSK9-D374Y mutant (2 μg/mL) was added, along with test compounds as indicated. Each sample was incubated for 16 h, whereupon the medium was replaced with fresh medium containing 10 μg/mL Bodipy FL LDL, and the samples were incubated for a further 4 h. Samples were then washed using warm PBS and LDL uptake was quantified on a EnVision Multimode Plate Reader (Perkin Elmer, Waltham, MA, USA) using excitation and emission wavelengths of 485 and 530 nm, respectively.

2.2.7. *Ex vivo* LDLR surface expression on primary human lymphocytes

Human peripheral blood mononuclear cells (PBMCs) were isolated from healthy human volunteers under protocols approved by the institutional ethics committee of Université de la Réunion using Ficoll Paque Plus. Human PBMCs were subsequently frozen at –80 °C in RPMI culture medium containing 70% FBS and 10% DMSO until use. Freshly thawed PBMCs were seeded into flat bottom 96-well plates (2 × 10⁵ cells per well) in RPMI containing 10 mM HEPES, 1 mM sodium pyruvate and 0.5% FCS for 2 h at 37 °C. The culture medium was subsequently supplemented with or without 600 ng/mL of recombinant PCSK9-D374Y for 4 h in the presence or absence of increasing concentrations of compound **3f** or alirocumab. Cells were subsequently washed with ice-cold PBS containing 1% BSA and then incubated with an allophycocyanin-conjugated antibody against human LDLR or an IgG1 isotype control for 20 min at room temperature away from light. Cell samples were washed twice in ice-cold PBS-1% BSA and once in ice-cold PBS prior to analysis on a CytoFLEX flow cytometer (Beckman Coulter, Pasadena, CA). Forward- versus side-scatter gates were set to include only viable lymphocytes and a minimum of 5 × 10³ lymphocytes were analysed for LDLR expression. The level of LDLR on the lymphocyte surface for each treatment condition was expressed as a % of the vehicle-only control that was unexposed to PCSK9-D374Y.

2.2.8. Pharmacokinetic studies

All pharmacokinetic studies were reviewed and approved by the Institutional Animal Care and Use Committee of ChemPartner (Shanghai, China). For 5-in-1 cassette dosing studies, male CD1 mice (31–32 g, 6–7 weeks) were acquired from LC Laboratory Animal Co. LTD and were allowed access to food and water *ad libitum* throughout the in-life phase of the study. Mice were dosed intravenously (IV) with a cassette of 0.4 mg/kg **1b**, **1c**, **1d**, **1g** and **3a** in 5% DMAC, 5% Solutol HS15 and 90% saline. At designated time points (0.083, 0.25, 0.5, 1, 2, 4, 8 and 24 h), mice were restrained manually when approximately 20 μL of blood was collected in K2EDTA tubes via the facial vein for serial bleeding or cardiac puncture (under anaesthesia with isoflurane) for terminal bleeding. Each blood sample was stored on wet ice until 20 μL of each sample was diluted with 60 μL deionised H₂O. Each sample was then vortexed well and then stored at –80 °C until analysis. Samples were assayed for their levels of **1b**, **1c**, **1d**, **1g** and **3a** by LC/MS/MS using an API 4000 triple Quadrupole system (Applied Biosciences, Foster City, CA USA) operating in a positive electrospray ionisation mode.

A second 5-in-1 cassette dosing study was conducted as described above with the following modifications: **2a**, **3c**, **3d**, **3e** and **3f** were analysed, CD1 mice were 28–29 g and 7–8 weeks of age and 20 μL of

each blood sample was diluted with 40 μ L deionised H₂O in preparation for analysis.

For a dedicated pharmacokinetic study of compound **3f**, male C57BL/6 mice (19–21 g) were purchased from LC Laboratory Animal Co. LTD and were given *ad libitum* access to food and water throughout the in-life phase of the study. Mice were dosed either IV with 5 mg/kg **3f** in 85% saline, 10% Solutol HS15 and 5% DMSO, orally (PO) with 20 mg/kg **3f** in 1% methylcellulose in H₂O or subcutaneously (SC) with 20 mg/kg **3f** in 85% saline, 10% Solutol HS15 and 5% DMSO. The animals were restrained manually at designated time points (0.033, 0.083, 0.25, 0.5, 1, 2, 4, 7 and 24 h) when approximately 110 μ L of blood was collected in K2EDTA tubes via retro orbital puncture for semi-serial bleeding or cardiac puncture (under anaesthesia with isoflurane) for terminal bleeding. Blood samples were placed on ice and centrifuged (2000 g, 5 min at 4°C) within 15 min of collection to obtain plasma samples which were subsequently stored at approximately –70 °C until analysis. Plasma samples were assayed for their levels of **3f** by LC/MS/MS using an API 5500 Qtriple system (Applied Biosciences) operating in a positive electrospray ionisation mode.

2.2.9. In vivo efficacy studies

The *in vivo* research protocol #2018040410477054 was approved by the animal use and care committee (CYROI). Female C57BL/6 wild-type and PCSK9^{-/-} knockout mice (8–16 weeks) were from Jackson Laboratory (Bar Harbor, NE, USA) and were housed in an accredited animal facility (20–25 °C, 50–80% humidity, 12 h light/dark cycles with access to standard chow and water *ad libitum*). Prior to dosing, mice acclimatised for 7 days with wild-type and PCSK9^{-/-} knockout mice caged separately (5 animals per cage). Mice were dosed SC daily for 14 days with either **3f** (3.28 mg/kg/day or 16.4 mg/kg/day in 5% DMSO and 95% saline) or vehicle only (5% DMSO and 95% saline). In

parallel, a separate cohort was dosed with evolocumab (10 mg/kg in 100% saline) once every 5 days. An *n* of 5 mice was used for each treatment group. On days 1, 5 and 10 of treatment, blood samples were collected from each animal via the retro-orbital plexus in a standard Eppendorf tube containing 1 μ L 0.5 M EDTA on ice. Samples were subjected to centrifugation at 2500 g, the plasma collected and then stored at –20 °C until analysis. On day 15, mice were humanely euthanised and blood collected and processed as described above. The abdominal cavity of each animal was dissected and visually inspected for signs of toxicity. All plasma samples were subsequently assayed for their total cholesterol and triglyceride levels using Cholesterol and Triglyceride FS colorimetric assay kits, respectively. Plasma samples were also analysed for their PCSK9 levels using a CircuLex mouse PCSK9 ELISA kit according to the manufacturer's instructions.

3. Results and discussion

3.1. The identification of a small organic molecule that disrupts the PCSK9-LDLR interaction

A major challenge associated with targeting the PCSK9-LDLR interaction with small molecules pertains to the relatively flat surfaces of the two interfaces involved (Fig. 1B and⁵). With this in mind, the catalytic domain of PCSK9 (Fig. 3A and PDB code 3P5C) was visually probed in the absence of the prodomain for sites proximal to the LDLR-binding interface that may accommodate the binding of a small molecular weight agent. It was surmised that an appropriately shaped small molecule binding within such a site may sufficiently disrupt the PCSK9-LDLR interface to inhibit association of the two proteins. On close inspection of the catalytic domain, it was noted that a groove normally occupied by the C-terminus of the prodomain and defined by residues

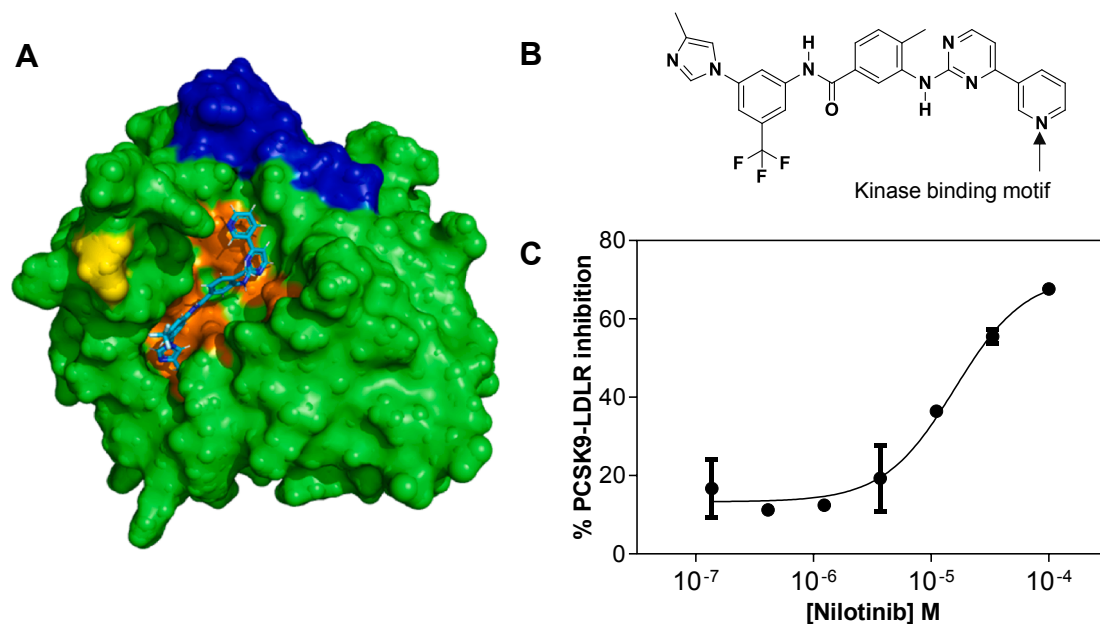


Fig. 3. Nilotinib is a small molecule inhibitor of PCSK9. (A) A molecular surface representation of the predicted interactions of nilotinib with the groove of PCSK9 leading into the enzyme's active site. The model was generated following a virtual screen of the BindingDB database²⁶ for compounds anticipated to interact with PCSK9 in the binding groove as defined in the Materials and Methods. Nilotinib is represented as a stick model with the carbon skeleton coloured in cyan while the molecular surface of the catalytic domain of PCSK9 is depicted in green. Amino acid residues that line the putative binding site are depicted in copper orange while the EGF-(A) LDLR-binding region of the PCSK9 is shown in blue. The residue highlighted in yellow is D212 and may provide a key interaction with analogues of nilotinib. The C-terminal domain of PCSK9 has been omitted for the purposes of clarity. (B) The chemical structure of nilotinib, emphasising one of its kinase binding motifs. (C) The inhibition of PCSK9 binding with LDLR by nilotinib shown as a function of drug concentration. Recombinant human His-tagged PCSK9 was mixed for 3 h at room temperature with varying concentrations of nilotinib (as designated) in microplates coated with the LDLR-EGF-AB domain and 1 × reaction buffer. The PCSK9-LDLR interaction was subsequently detected using a colorimetric-based assay as detailed in the Materials and Methods. Panel (C) is a single example of seven independent experiments, with the error bars representing the S.D. of duplicates within this example.

His 226, Leu 230, Leu 253, Thr 264, Leu 286, Leu 289, Ala 290, Leu 297, Asn 317 and Ser 386 (Fig. 3A and Supplementary Fig. S1) may potentially satisfy these requirements. In an effort to identify a compound of this nature, an *in silico* screen of the FDA-approved small molecule collection in BindingDB was deployed.²⁶ The screen yielded 10 theoretical candidates which included nilotinib (Fig. 3B). Fig. 3A depicts a computational docking pose of nilotinib bound within the nominal binding groove of PCSK9 (with some residues omitted for clarity) and is proximal to the EGF(A)-binding surface and catalytic triad of the protein. Nilotinib was sourced from a commercial vendor and subsequently assayed for inhibition of the PCSK9-LDLR interaction using an *in vitro* binding assay. The assay confirmed that nilotinib was a bona fide inhibitor of the PCSK9-LDLR interaction with an assay IC₅₀ of approximately 15.9 μM (Fig. 3C). The result was robust with the drug demonstrating an average assay IC₅₀ of 9.8 μM, a value that was derived from seven independent experiments (IC₅₀ range 3.9 – 15.9 μM, Table 1).

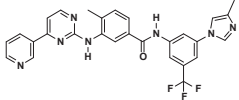
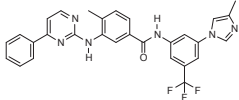
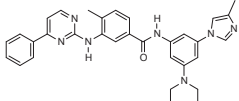
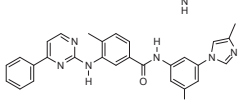
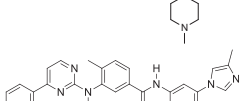
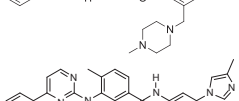
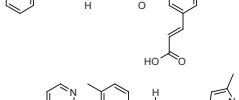
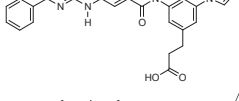
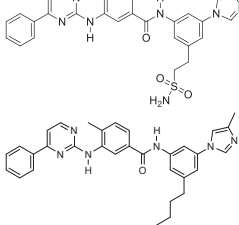
3.2. Medicinal chemistry campaign

3.2.1. Series 1

Given that nilotinib is a marketed Bcr-Abl inhibitor (Tasigna®) and possessed unwanted kinase activity, the next phase of discovery focused on minimizing off-target kinase inhibition while maintaining or improving activity in the PCSK9-LDLR binding assay. In the first round of optimization, removal of the kinase binding moiety (Fig. 3B) and early substitutions of the trifluoromethyl group of nilotinib (Fig. 3B) sharply reduced kinase inhibitory activity against a small panel of kinases represented by Src, c-Kit, Abl and PDGFR-β (Table 1), while maintaining or increasing potency in the PCSK9-LDLR binding assay (Table 1). It should be noted that PDGFR-β, c-Kit and Abl were selected as they represent a sub-set of kinases particularly susceptible to inhibition by nilotinib³¹ and are therefore ideal proxies for analysing any undesirable kinase inhibitory activity retained by compounds generated in this campaign. While Src is relatively impervious to inhibition by

Table 1

The chemical structures of nilotinib, compounds **1a–1h** and associated IC₅₀ (μM) values as determined by an *in vitro* PCSK9-LDLR binding assay and *in vitro* c-Kit, Abl, PDGFR-β or Src kinase assays. Each assay was performed once unless otherwise specified as described in the Materials and Methods. ID indicates identifier.

ID	Structure	PCSK9-LDLR IC ₅₀ (μM)	Kinase assay IC ₅₀ (μM)			
			c-Kit	Abl	PDGFR-β	Src
Nilotinib		9.8 (range 3.9–15.9, n = 7)	0.158	0.0012	0.025	1.9
1a		8.4	0.592	0.334	2.48	> 10
1b		0.491	1.49	7.95	1.51	4.36
1c		0.758	2.88	> 10	> 10	> 10
1d		0.714	2.57	> 10	5.42	> 10
1e		11.3	2.77	> 10	> 10	> 10
1f		9.28	0.347	> 10	> 10	> 10
1g		13.4	6	> 10	> 10	> 10
1h		7.41	0.302	0.142	> 10	> 10

nilotinib³¹, it was selected as a representative of the Src family of tyrosine kinases. Inhibition of members of this family by any given compound can generate clinically deleterious side-effects.³² Exchange of the pyridine ring present in nilotinib for an unsubstituted phenyl (**1a–1h**, Table 1) consistently reduced kinase inhibitory activity across the series, with certain examples showing only micromolar inhibition of c-Kit. At the same time, the most potent antagonists of the target protein–protein interaction bore basic substitutions off the right-hand phenyl ring *meta* to the imidazole (**1b–1d**, Table 1), all of which achieved sub-micromolar activity. Acidic or non-basic hydrophilic groups (**1e–1g**, Table 1) were effectively no more potent than nilotinib itself, although they were consistently less active against Abl, PDGFR- β and Src kinases. Abl-inhibitory activity returned in the case of the neutrally substituted example **1h** (Table 1).

3.2.2. Series 2

With this encouraging early SAR in hand, the next phase of exploration sought to probe changes in three disparate portions of the molecule to promote affinity for PCSK9, minimise anti-kinase activity and improve on any perceived ADME liabilities (Fig. 4A). First, it was

rationalised that the introduction of a fluorine atom at position X of Fig. 4A may endow greater metabolic stability by inhibiting possible aromatic ring metabolism. Second, modelling of compound **1d**'s basic piperazinomethylene moiety indicated a potential interaction through the acidic side-chain of Asp 212 of PCSK9 that could be exploited further in this series (Figs. 3A, 4B and Supplementary Fig. S1). Third, only modest variations around the imidazole group (Fig. 4A) were probed as modelling suggested that any substituent off the right hand 5-membered heterocycle larger than a methyl group would not favour binding (data not shown). Table 2 indicates the results of this series.

The introduction of a fluoro substituent at the *para* position of the left-hand phenyl ring (e.g. compound **2a**) was insignificant in the context of PCSK9-LDLR inhibition (Table 2). That some inhibition of certain kinases at sub-10 μ M levels remained (compounds **2a**, **2c–2f**) may be attributable to other pharmacophores (Table 2). There are multiple examples of morpholine- and aminopyrimidine-based hinge-binding motifs³³ so it is not possible to rule out such orientations of compounds in this series for interactions with c-Kit, for example (Table 2).

Consistent with the modelling of compound **1d** and a putative

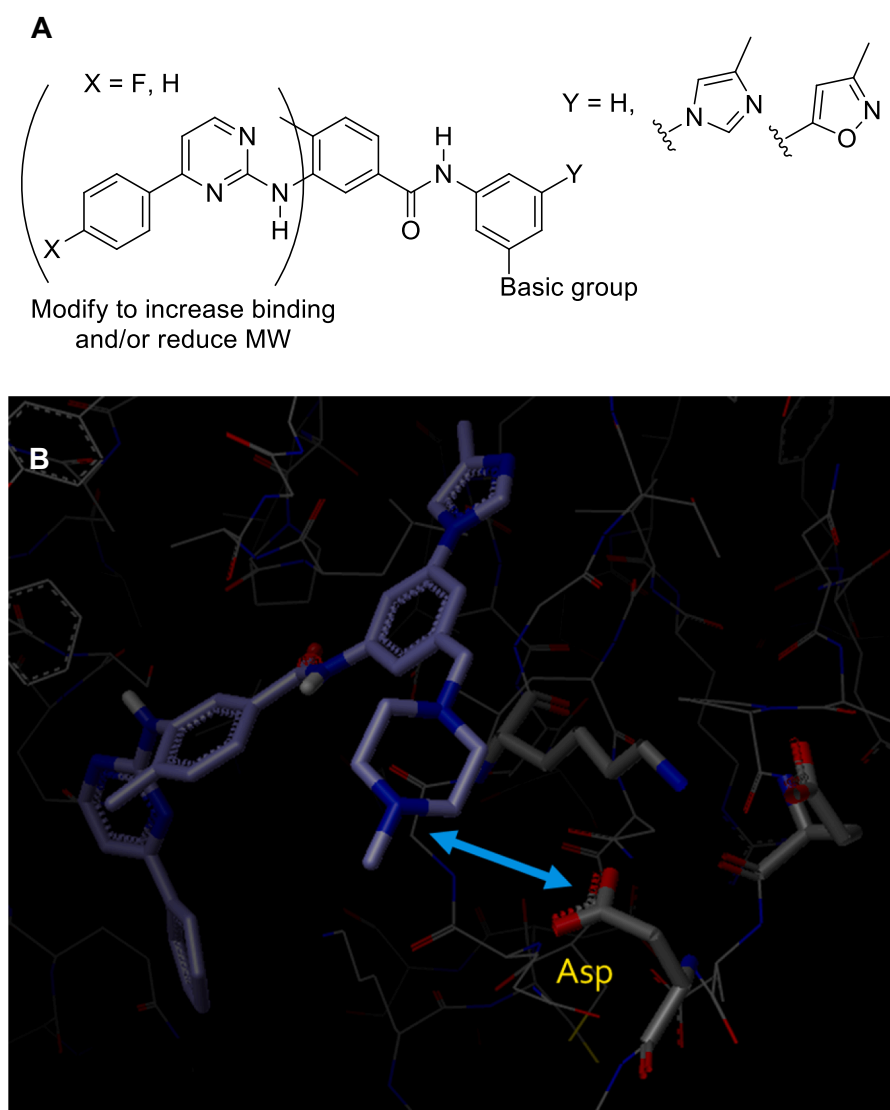
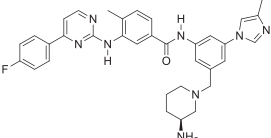
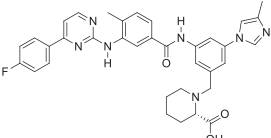
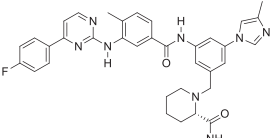
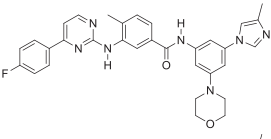
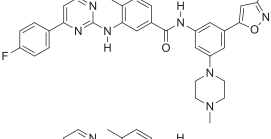
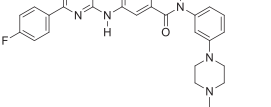


Fig. 4. (A) A molecular scaffold showing where changes to the molecule were designed to afford increased affinity for PCSK9 along with decreased off-target selectivity and improved drug-like properties. (B) A molecular model of compound **1d** docked into the putative binding site of PCSK9. In this model, the basic piperazinomethylene moiety of compound **1d** is proximal to the acidic side-chain of Asp 212 of PCSK9 (indicated in yellow), potentially enabling a stabilising interaction to occur (indicated by a light blue double-headed arrow).

Table 2

The chemical structures of compounds **2a–2f**. The IC₅₀ value (μM) of each compound was evaluated in either an *in vitro* PCSK9-LDLR binding assay or an *in vitro* c-Kit, Abl, PDGFR-β or Src kinase assay. Each assay was conducted once as described in the Materials and Methods. ID indicates identifier. An asterisk denotes an IC₅₀ value that was obtained over a suboptimal assay dynamic range, due perhaps to physical compound characteristics (e.g. solubility).

ID	Structure	PCSK9-LDLR IC ₅₀ (μM)	Kinase assay IC ₅₀ (μM)			
			c-Kit	Abl	PDGFR-β	Src
2a		0.428*	1.96	> 10	2.04	> 10
2b		14	> 10	> 10	> 10	> 10
2c		2.57	9.87	> 10	> 10	> 10
2d		40.1	0.79	> 10	> 10	> 10
2e		10.7	3.1	> 10	5.52	> 10
2f		3.29*	0.093	> 10	> 10	> 10

interaction of its piperazinomethylene moiety with Asp 212 of PCSK9 shown in Fig. 4B, the requirement for a distal basic group extending from the right-hand phenyl ring to achieve potency was clear from this exercise. Like the potency displayed by piperazine-bearing compounds **1b–1d** (Table 1), compound **2a** displayed sub-μM inhibition of the PCSK9-LDLR interaction (Table 2), most likely because of the basic nature of its aminopiperidine group. In contrast, compounds **2b–2d**, while retaining the piperidine group of **2a** yet decorated with various appendages from the six-membered ring, lost substantial potency relative to **2a** in the binding assay (Table 2). Compound **2c**, (IC₅₀ = 2.57 μM, Table 2) was a possible exception, perhaps due to a non-ionic hydrogen bond interaction between the Asp 212 side-chain of PCSK9 (Fig. 4B) and **2c**'s amide group, but this was not verified.

Substitution of the imidazole in **1c** with a methylisoxazole group having similar geometry yet different charge potential cost approximately a log in potency in the PCSK9-LDLR binding assay (compound **2e**, Table 2), pointing to the need for the basic nitrogen. The flanking methyl group was retained not so much for physical interaction but to minimize the potential for heme binding/CYP450 enzyme interaction. Removal of the imidazole from **1c** altogether (**2f**, Table 2) served to reduce PCSK9-LDLR binding somewhat, and reintroduced a degree of kinase inhibition, perhaps via the aforementioned aminopyrimidine type pharmacophore.³³

3.2.3. Series 3

The next phase of optimization explored core modifications as well

as truncating the left-hand side of the molecule, to lower molecular weight, to decrease the chance of alternative kinase binding modes, and to enhance novelty (Fig. 4A). With this in mind, we retained the methylimidazolyl-phenyl group and basic moieties on the right-hand side of the molecule that were crucial for maintaining sub-μM binding against PCSK9-LDLR (Table 3). This series clearly demonstrated the benefit of smaller left-hand groups in avoiding off-target (kinase) inhibition (Table 3). While PCSK9-LDLR binding was substantially reduced in the case of the toluamide **3b** relative to the comparator **1c**, this compound showed no sub-10 μM kinase inhibition in the small panel (Table 3). The aryl ketone **3e** behaved similarly, though with improved target binding (Table 3).

Replacement of the aminopyrimidine linker with aryl ethers (**3c**, **3d**, and **3f**, Table 3) illustrated the most favourable potency and selectivity numbers thus far. Noteworthy was the isoquinoline ether **3d**, which yielded the most potent small molecule inhibition of PCSK9-LDLR yet observed (IC₅₀ = 78 nM, Table 3), albeit across a narrow dynamic range that could have been limited by physical compound characteristics. The selectivity was also less for **3d** against the kinase panel (Table 3), perhaps due to kinase hinge binding *via* the isoquinoline nitrogen.

3.3. A summary of the medicinal chemistry campaign

Collectively, the results indicate that potency against the PCSK9-LDLR interaction is likely driven both by favourable basic groups

Table 3

The structures of compounds **3a–3f**. Compounds were assayed for inhibition of the LDLR-PCSK9 interaction using an *in vitro* binding assay as described in the Materials and Methods. In parallel, each compound was also evaluated for inhibition of c-Kit, Abl, PDGFR- β or Src activity using an *in vitro* kinase assay as detailed in the Materials and Methods section. Values represent the assay IC₅₀ (μ M) of each compound obtained from a single experiment. ID indicates identifier. An asterisk denotes that the IC₅₀ value was obtained over a suboptimal assay dynamic range as described in the legend of Table 2.

ID	Structure	PCSK9-LDLR IC ₅₀ (μ M)	Kinase assay IC ₅₀ (μ M)			
			c-Kit	Abl	PDGFR- β	Src
3a		13.4	0.618	> 10	> 10	> 10
3b		26.3	> 10	> 10	> 10	> 10
3c		0.759*	> 10	> 10	7.66	> 10
3d		0.078*	0.227	> 10	3.29	2.62
3e		2.13	> 10	> 10	> 10	> 10
3f		0.537	> 10	> 10	> 10	> 10

(Tables 1 and 2) combined with linked biaryl ethers (Table 3). The phenoxyphenyl ethers (compounds **3c** and **3f**, Table 3) provide an ideal balance between potency and selectivity. The isoquinoline group's added potency (compound **3d**, Table 3) is consistent with a further potential interaction between the ring nitrogen and the side-chain of Lys 222 within the binding pocket of PCSK9 (Supplementary Figs. S1 and S2). Supplementary Fig. S2 shows that the angular methyl group on the interior ring places the distal aromatic in a favourable tilt, resulting in a sub-3 Å distance between side chain and inhibitor groups.

3.4. Compound **3f** binds directly to PCSK9

While compound **3f** (and the entire chemical series in general) was designed to bind within the putative binding site of PCSK9 (Fig. 3A), it remained conceivable that disruption of the target protein–protein interaction was mediated through direct antagonism of LDLR as opposed to PCSK9. In an effort to confirm direct binding of compound **3f** to PCSK9, biolayer interferometry analysis of the interaction was deployed. The anti-PCSK9 monoclonal antibody evolocumab³⁴ was initially captured by an Anti-hIgG Fc Capture (AHC) biosensor and then exposed to varying concentrations of PCSK9. Fig. 5A demonstrates that

PCSK9 readily associated with evolocumab in a concentration-dependent manner at low doses (1.56–50 nM) of the protein, consistent with a very tight interaction ($K_D = 8.0$ pM,³⁵). The interaction was also highly stable, with no clear loss of PCSK9 binding detectable in the first 10 min of dissociation (Fig. 5A). Next, biotinylated PCSK9 was loaded onto a Super Streptavidin (SSA) biosensor and then exposed to increasing concentrations of compound **3f**. While no binding was evident at 0.2 and 0.4 μ M **3f** (Fig. 5B), a clear increase in biolayer interferometry shift was notable at 0.8 and 1.6 μ M **3f** (Fig. 5B), indicating direct binding by compound **3f** to PCSK9. It is important to note that non-specific binding by the compound was eliminated by subtracting background signal. Moreover, investigations are ongoing to further confirm this preliminary data.

3.5. Compounds **1c**, **3d** and **3f** restore LDL uptake by HepG2 liver cells in the presence of PCSK9 D374Y

Next, selected compounds were subjected to a cell-based assay to evaluate their impairment of the PCSK9-LDLR interaction in a functional context. Human liver HepG2 cells expressing LDLR at their plasma membrane were incubated with the gain-of-function mutant PCSK9 D374Y (Fig. 1A and^{1,3}) either alone or in combination with compounds **1c**, **3c**, **3d** or **3f**. AMB-657286, a small molecule inhibitor of the PCSK9-LDLR interaction developed by Shifa Biomedical,³⁶ was used as a reference control. As anticipated, PCSK9 D374Y significantly impaired the uptake of fluorescently labelled LDL particles by HepG2 liver cells relative to an untreated control (Fig. 5C). Fig. 5C shows that co-incubation with 0.1 or 1 μ M of the reference compound AMB-657286 relieved the inhibition of uptake by PCSK9 D374Y, with LDL uptake returning to baseline levels at 1 μ M. On the addition of 0.1 or 1 μ M **1c**, **3d** or **3f**, there was a dose-dependent restoration of LDL internalization by liver cells to baseline levels (Fig. 5C), suggesting that these compounds disrupted the target protein–protein interaction. Compound **3c** was the exception of this group, with the compound displaying no significant increase in LDL uptake by liver cells (Fig. 5C). It is noteworthy that compounds **1c**, **3d** and **3f** maintain activity through the restoration of LDL uptake even though the gain-of function mutant PCSK9 D374Y applied in this assay binds 6–25-fold more potently with LDLR relative to its wild-type counterpart.^{37,38}

In an effort to rationalise why **3c** had achieved sub- μ M potency in the PCSK9-LDLR binding assay (Table 3) yet failed to increase LDL cellular uptake (Fig. 5C), we re-examined its potency in the binding assay. As mentioned earlier, the dynamic range of the binding assay was relatively narrow for some compounds, for reasons not yet determined. In particular, **3c** showed a maximum inhibition of 20% in this assay, whereas compounds **1c**, **3d**, and **3f** all showed at least 35% inhibition, with **3f** showing 57% inhibition at the highest concentration tested (data not shown). It was therefore concluded that potency in the biochemical binding assay served as a useful surrogate for cell-based restoration of LDL uptake presuming the range of inhibition was at least 35%. To date we have not established upper and lower limits of the binding assay's utility, other than to conclude that 20% is insufficient to translate to cellular efficacy.

It is also noteworthy that compound **3f** restored LDL uptake by HepG2 cells at a dose (0.1 μ M, Fig. 5C) that was lower than its IC₅₀ as evaluated by the *in vitro* PCSK9-LDLR binding assay (0.537 μ M, Table 3). While the *in vitro* binding assay data is consistent within the chemical series detailed in Tables 1–3, this biochemical assay cannot fully account for any indirect mechanisms that may confer activity in cellular assays such as the HepG2 assay (Fig. 5C). A variety of factors operating beyond the immediate control of the experimental conditions in more complex cellular systems may explain the discrepancy between effects observed at lower concentrations than those predicted by the biochemical assay. Whether these be additional molecular targets and/or physicochemical characteristics with effects on permeability etc, we are working to clarify these as we develop this series further.

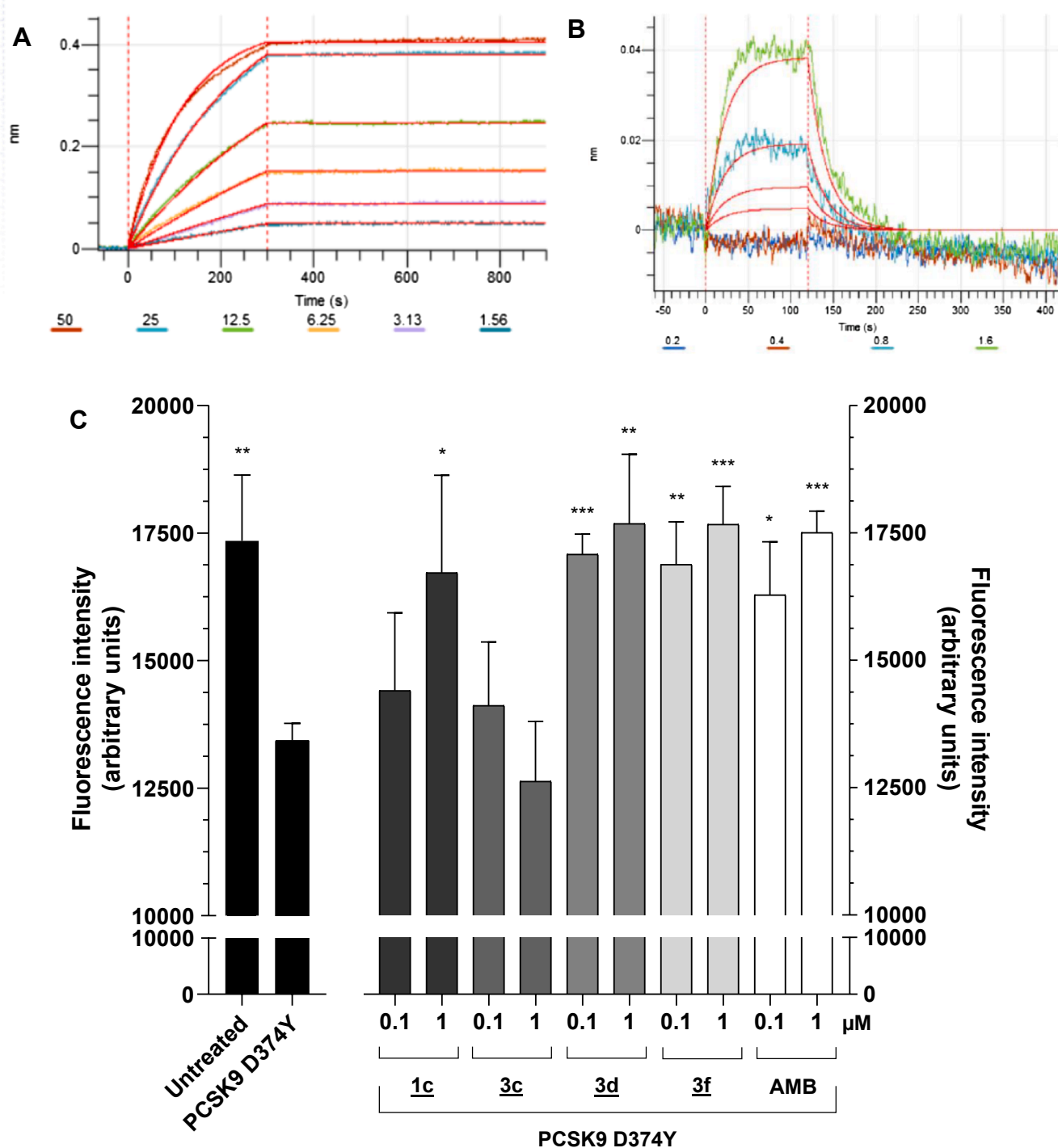


Fig. 5. Evolocumab and compound **3f** bind directly to PCSK9. Bi-layer interferometry analysis of evolocumab or compound **3f** binding with PCSK9 using a ForteBio Octet® RED96 system. (A) Evolocumab was immobilized to an Anti-hIgG Fc Capture (AHC) biosensor and then exposed to various concentrations of PCSK9 (1.56–50 nM as indicated) for 5 min. The interaction was subsequently allowed to dissociate for a period of 10 min. (B) Biotinylated PCSK9 was captured by a Super Streptavidin (SSA) biosensor and then exposed to compound **3f** at a variety of concentrations (0.2–1.6 μM as denoted) for 2 min. Compound **3f** was then permitted to dissociate for a further 10 min. Each sensogram exhibits the bi-layer interferometry signal (nm) expressed as a function of time (s). (C) Compound **3f** promotes the uptake of fluorescently labelled LDL by human liver HepG2 cells in the presence of PCSK9 D374Y. HepG2 cells were co-incubated with the gain-of-function PCSK9 D374Y mutant (2 μg/mL) and compounds **1c**, **3c**, **3d**, **3f** or AMB (0.1 or 1 μM) as indicated for 16 h. Fluorescently labelled LDL (10 μg/mL) was subsequently added for 4 h prior to the measurement of LDL uptake by HepG2 cells as detailed in the Materials and Methods. Each column represents the average cellular uptake of LDL as indicated by the fluorescence in arbitrary units. Error bars represent the S.D. of triplicates. An unpaired student *t* test (two-tailed) was applied to each sample using the PCSK9 D374Y only control as a comparator. *P* values < 0.05 are designated with asterisks: *** < 0.001, ** < 0.01, * < 0.05. “AMB” denotes the compound AMB657286.

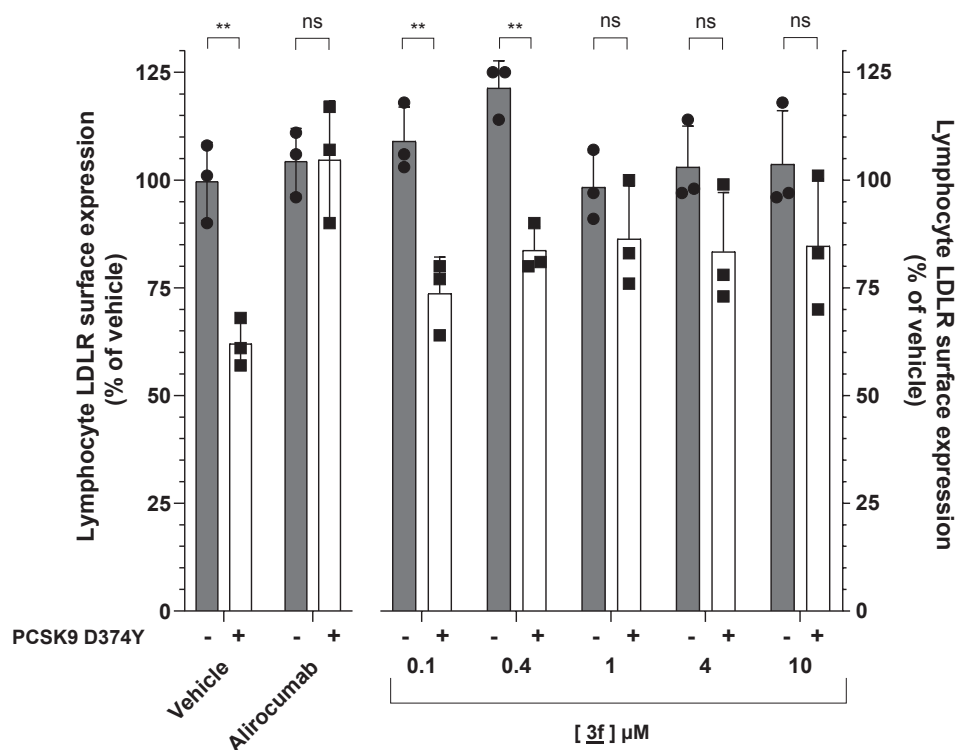


Fig. 6. Compound **3f** restores the expression of LDLR on the cellular surface of human lymphocytes in the presence of mutant PCSK9-D374Y. Human PBMCs were cultured in the presence or absence of 600 ng/mL recombinant PCSK9-D374Y along with increasing doses of compound **3f** or alirocumab for 4 h. Cell samples were washed with ice-cold PBS/1% BSA and then incubated with an allophycocyanin-conjugated α -LDLR antibody at room temperature for 20 min. Following $2 \times$ ice-cold PBS/1% BSA washes and a final wash with ice-cold PBS, samples were analysed by flow cytometry as detailed in the Materials and Methods. Each column represents the average level of LDLR on the surface of lymphocytes relative to the untreated control which was normalized to 100%. Error bars represent the S.D. of triplicates. An unpaired student *t* test (two-tailed) was applied to each treatment pair. *P* values < 0.05 are designated with asterisks: ** < 0.01, ns denotes not significant.

Table 4

A summary of the *in vitro* IC₅₀ values (μ M) of select compounds from Tables 1–3 presented alongside their pharmacokinetic properties in male CD1 mice. Mice were dosed once (0.4 mg/kg) IV with a 5-in-1 cassette of either **1b**, **1c**, **1d**, **1g** and **3a** or **2a**, **3c**, **3d**, **3e** and **3f**. Blood samples were collected at designated timepoints (0.033, 0.083, 0.25, 0.5, 1, 2, 4, 7 or 8 and 24 h) and then processed for analysis by LC/MS/MS to evaluate their compound levels. Pharmacokinetic parameters are designated as follows: CL, clearance of compound; V_{ss}, volume of distribution at equilibrium; T_{1/2}, terminal half-life; AUC_{last}, area under the blood concentration–time curve from t = 0 to the last measurable timepoint; AUC_∞, area under the blood concentration–time curve from t = 0 to infinity, MRT_∞, mean residence time extrapolated to infinity.

ID	PCSK9-LDLR IC ₅₀ (μ M)	Kinase assay IC ₅₀ (μ M)				IV PK data from cassette studies					
		c-Kit	Abl	PDGFR- β	Src	CL (L/h/kg)	V _{ss} (L/kg)	T _{1/2} (h)	AUC _{last} (h*ng/mL)	AUC _∞ (h*ng/mL)	MRT _∞ (h)
1b	0.491	1.49	7.95	1.51	4.36	3.15	3.74	1.64	116	127	1.19
1c	0.758	2.88	> 10	> 10	> 10	1.97	4.3	2.21	189	204	2.16
1d	0.714	2.57	> 10	5.42	> 10	2.14	5.65	3.29	166	187	2.66
1g	13.4	6	> 10	> 10	> 10	6.58	1.72	0.216	58.5	63.7	0.239
3a	13.4	0.618	> 10	> 10	> 10	0.748	1.69	2.15	508	541	2.27
2a	0.428*	1.96	> 10	2.04	> 10	1.41	13.3	10.8	243	297	10.4
3c	0.759*	> 10	> 10	7.66	> 10	1.05	9.26	7.36	338	384	8.98
3d	0.078*	0.227	> 10	3.29	2.61	3.05	6.7	2.77	128	133	2.3
3e	2.13	> 10	> 10	> 10	> 10	4.86	4.7	1.09	78	83	0.96
3f	0.537	> 10	> 10	> 10	> 10	0.3	9.13	25.7	722	1472	34.9

3.6. Compound **3f** restores the expression of LDLR on the cellular surface of human lymphocytes in the presence of mutant PCSK9 D374Y

While compounds **1c**, **3d** and **3f** promoted the uptake of LDL by HepG2 cells despite the presence of mutant PCSK9-D374Y, further evidence was sought to establish the compounds' mechanism of action as inhibitors of the PCSK9-LDLR interaction. It is well established that PCSK9 functions to direct the LDLR for lysosomal degradation following endocytosis by hepatocytes, thereby preventing LDLR recycling to the cell surface.^{10,11} Consistent with this notion, the addition of exogenous PCSK9 D374Y to primary human lymphocytes in an *ex vivo* system³⁹ significantly decreased the surface expression of LDLR by ~40% relative to untreated controls (Fig. 6). The co-addition of alirocumab, a humanized monoclonal antibody against PCSK9⁴⁰, completely relieved the suppression of LDLR expression induced by PCSK9 D374Y (Fig. 6), a result that validates the assay as appropriate for the detection of PCSK9 inhibition. On the introduction of 0.1 and 0.4 μ M compound **3f**

alongside PCSK9 D374Y, there was no evidence of restoration of LDLR expression on the surface of lymphocytes relative to controls that did not receive the mutant PCSK9 D374Y (Fig. 6). However, higher doses of **3f** (1–10 μ M) did indeed rescue LDLR levels (Fig. 6), to a point where **3f**- and PCSK9 D374Y-treated samples were not significantly different from their PCSK9-untreated counterparts. Collectively, these results indicate that compound **3f** at 1–10 μ M rescues LDLR from PCSK9-mediated destruction, thereby enabling a restoration of receptor levels at the cell surface.

3.7. A pharmacokinetic evaluation of compound **3f** and analogues

As a prelude to *in vivo* efficacy studies, the most potent compounds were subsequently screened using a murine cassette-based pharmacokinetic system to evaluate their clearance, half-life and volume of distribution parameters. Following IV administration with selected compounds, blood was sampled from male CD1 mice (0–24 h) and then

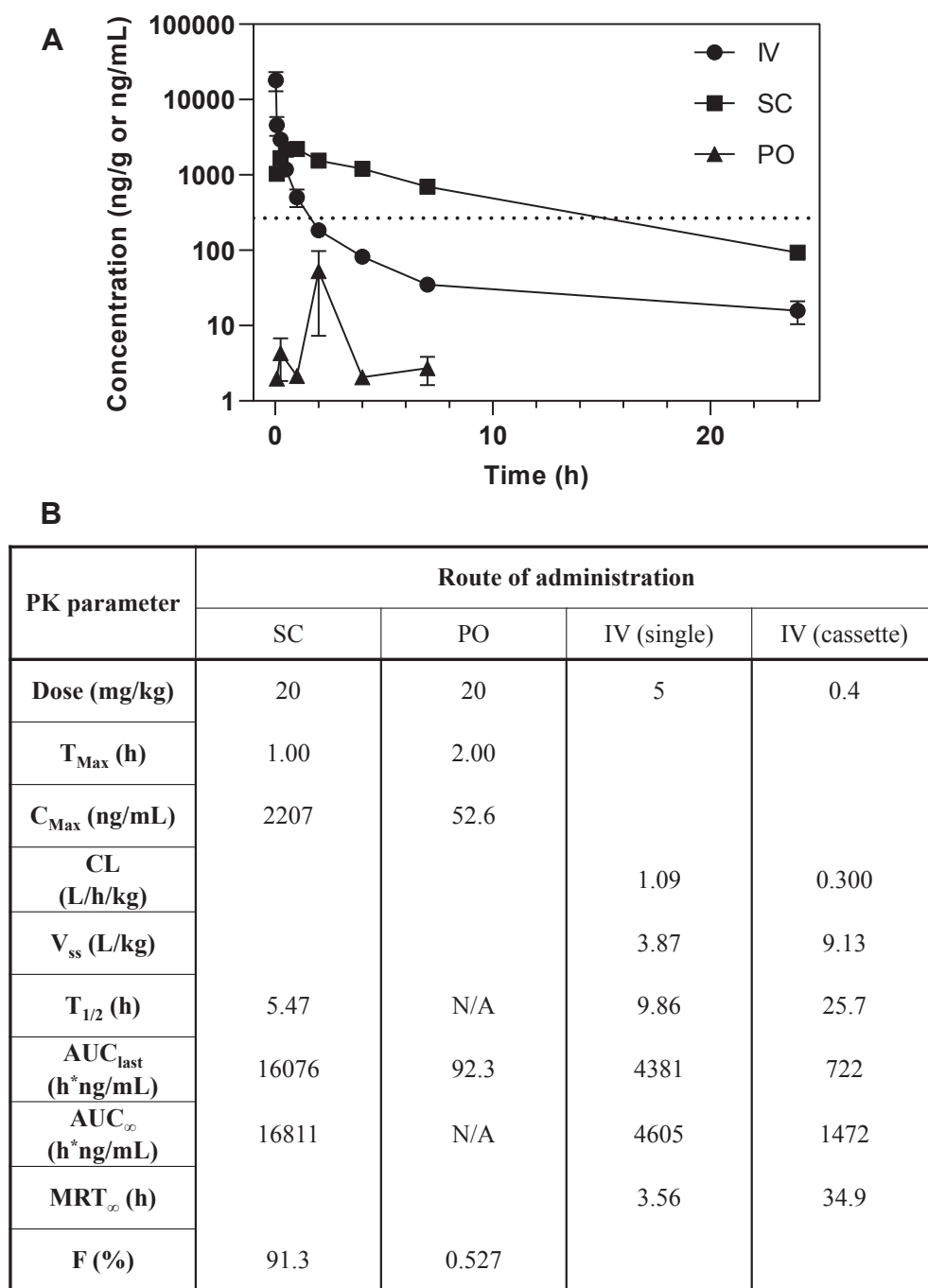


Fig. 7. (A) The average plasma concentrations of compound **3f** in male C57BL/6 mice following a single dose via the following routes: IV at 5 mg/kg (circles), SC at 20 mg/kg (squares) or PO at 20 mg/kg (triangles). Mice were dosed and blood samples collected at $t = 0.083, 0.25, 0.5, 1, 2, 4, 7$ and 24 h. Samples were processed and analysed for their levels of **3f** as described in the Materials and Methods. Plasma concentrations are shown as a function of time ($n = 3$ per administration arm). Error bars represent the S.D. of three individual replicates. The dotted line running parallel with the x-axis indicates the average IC_{50} of compound **3f** as evaluated in the PCSK9-LDLR binding assay and is taken from Table 1. (B) The pharmacokinetic properties of **3f** as calculated using the data presented in panel (A). The data obtained from dosing **3f** as part of an IV cassette was taken from Table 4 and is presented here for the purposes of comparison. Pharmacokinetic parameters are designated as described in the legend of Table 4 and as follows: C_{Max} , the maximum blood concentration achieved by the compound; T_{Max} , the time at which C_{Max} occurs; F , the fraction of compound that is bioavailable.

evaluated for levels of parent compound. Table 4 summarises the pharmacokinetic values of each compound screened.

The first round of studies (represented in the top half of Table 4) established that compounds bearing a truncated phenoxyphenyl core (e.g. compound **3a**, Table 4) were likely to be cleared less rapidly than aminopyrimidines (**1b–1d** and **1g**, Table 4). While **3a** did not show sufficient potency against the PCSK9-LDLR target ($IC_{50} = 13.4 \mu M$, Table 4) its low clearance and mean residence time (0.748 L/h/kg and 2.27 h, respectively, Table 4) suggested that the more potent and selective analogue **3f** might behave accordingly. Indeed, when dosed in the second round (indicated by compounds in the bottom half of Table 4), **3f** proved to be superior in all aspects, with potential for once per day dosing as suggested by an extended half-life ($T_{1/2} = 25.7$ h, Table 4) and low clearance (CL = 0.3 L/h/kg, Table 4).

To further evaluate the pharmacokinetic properties of **3f**, cassette studies were followed by a dedicated bioavailability study of **3f** via oral, intravenous and subcutaneous routes. The pharmacokinetic profile and parameters of male C57BL/6 mice dosed with **3f** via these routes is presented in Fig. 7. While **3f** was not well absorbed orally (Fig. 7) the compound demonstrated excellent bioavailability via subcutaneous administration (91%, Fig. 7) and was judged suitable for *in vivo* proof-of-concept studies.

In addition to its high subcutaneous bioavailability, it was noted that the plasma concentrations of **3f** in mice treated SC with 20 mg/kg **3f** exceeded the PCSK9-LDLR binding inhibition IC_{50} value of 537 nM (Table 3) over at least 16 h (horizontal dotted line, Fig. 7), with 24 h concentrations at approximately 93 nM. Notionally, this may translate to potential once-a-day dosing at 20 mg/kg/day for proof-of-concept

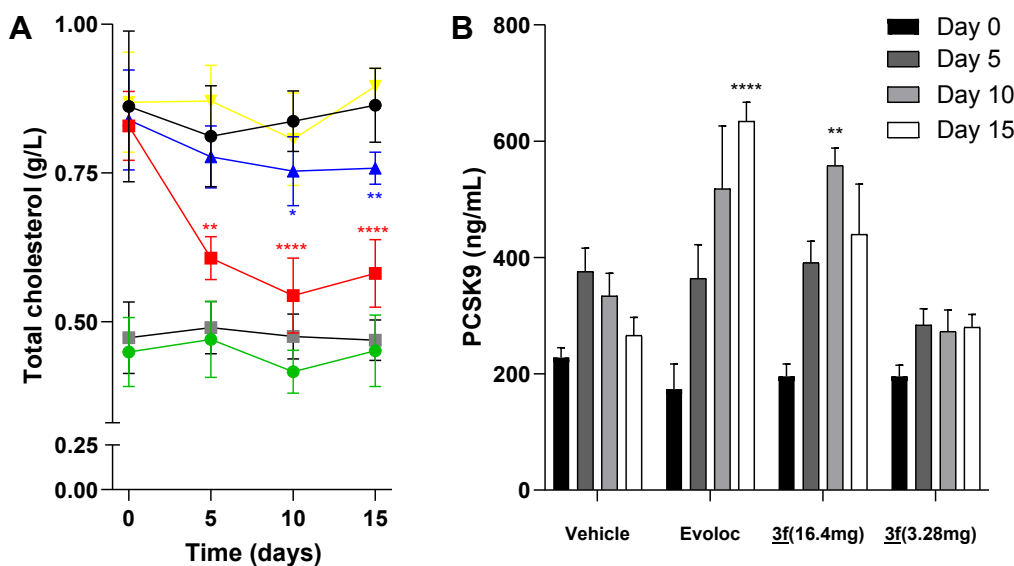


Fig. 8. (A) The average total cholesterol plasma levels (g/L) of female C57BL/6 wild-type mice treated SC daily for 14 days with either vehicle (black circles) or **3f** (3.28 or 16.4 mg/kg/day, inverted yellow triangles and blue triangles, respectively) shown as a function of time. In parallel, a separate cohort was dosed with evolocumab (10 mg/kg in 100% saline) once every 5 days (red squares). Female PCSK9^{-/-} knockout mice were also treated in parallel with vehicle (green circles) or 16.4 mg/kg/day **3f** (grey squares) as indicated ($n = 5$ per treatment group). Error bars represent the S.D. of 5 replicates. An unpaired student t test (two-tailed) was applied to each sample within the evolocumab and **3f** (16.4 mg/kg/day) treated test groups using the equivalent vehicle only control as the comparator. P values < 0.05 are designated with asterisks: **** < 0.0001 , ** < 0.01 , * < 0.05 . (B) A subset of the

plasma samples described in (A) were concurrently assayed for their total PCSK9 levels. Each column represents average PCSK9 plasma levels (ng/mL) as a function of time (0, 5, 10 and 15 days as indicated) and are grouped according to their treatment as detailed in (A). “Evoloc” indicates the cohort treated with 10 mg/kg evolocumab every 5 days while “**3f** (16.4 mg)” and “**3f** (3.28 mg)” designate groups that were treated with 16.4 or 3.28 mg/kg/day **3f**, respectively. Error bars represent the SEM of 5 replicates. An unpaired student t test (two-tailed) was applied to each sample using the equivalent vehicle only control as a comparator. P values < 0.05 are designated with asterisks: **** < 0.0001 , ** < 0.01 .

studies, although there is also the possibility of drug accumulation over several days. With this in mind, a lower dose regimen (4 mg/kg/day) was incorporated into proof-of-concept studies alongside 20 mg/kg/day².

3.8. Compound **3f** lowers total cholesterol levels in the plasma of wild-type mice

Wild-type mice are often considered to be sub-optimal as models for LDL-c-lowering therapies as the majority of their total plasma cholesterol is carried as HDL-c (80–90%) with a low fraction incorporated as LDL-c^{41,42}, a profile that is typically inverted relative to the human state. Despite this limitation, the use of wild-type mice is appropriate in this context as HDL-c levels (and by proxy, total cholesterol levels) are modulated by the LDLR as they contain apolipoprotein E, a ligand for the LDLR⁴³. Moreover, the putative binding site of compound **3f** is fully conserved between human, mouse and other mammalian forms of PCSK9 (Supplementary Fig. S1), making cross-species testing feasible.

In an effort to validate wild-type mice as an appropriate *in vivo* model, female C57BL/6 wild-type mice were treated SC with evolocumab (10 mg/kg every 5 days). Fig. 8A demonstrates that evolocumab decreased total cholesterol plasma levels by ~30% relative to vehicle-only controls on the final day of the experiment. Since evolocumab is an FDA-approved monoclonal antibody raised against PCSK9 and used to lower LDL-c in humans with hypercholesterolemia,³⁴ it can be concluded that the murine model was appropriate for the detection of agents that lower LDL-c levels. In parallel, mice treated with 3.28 mg/kg/day **3f** exhibited no decrease in total cholesterol (Fig. 8A), however a cohort exposed to 16.4 mg/kg/day **3f** displayed a modest yet significant decrease in total cholesterol plasma levels of ~10% (Fig. 8A). In a result consistent with literature values,⁴⁴ PCSK9 knockout mice demonstrated typically low cholesterol levels throughout the time course of the experiment (Fig. 8A). Notably, PCSK9^{-/-} mice treated with 16.4 mg/kg/day **3f** did not exhibit any further decrease in total cholesterol relative to vehicle-only treated PCSK9^{-/-} controls (Fig. 8A),

suggesting that the decrease of ~10% observed in the wild-type cohort treated with 16.4 mg/kg/day **3f** was mediated via a PCSK9-dependent mechanism. The levels of circulating triglycerides were largely unaffected by any treatment (Supplementary Fig. S3). It should be noted that no change in mouse body weight in any treatment cohort was observed nor was there any change in behaviour for each experimental group (data not shown).

While 5 days in-life is sufficient for evolocumab to achieve a decrease in total cholesterol (Fig. 8A), a longer period was required for compound **3f** at 16.4 mg/kg/day to significantly reduce total cholesterol in mice plasma (day 10, Fig. 8A). This can readily be explained by the antibody's improved pharmacological profile (e.g. likely a greater affinity for PCSK9, [compare Fig. 5A and B]) relative to that of the small molecule inhibitor **3f**. That compound **3f** required 10 days of in-life treatment at 16.4 mg/kg/day to induce a statistically significant decrease in total cholesterol (Fig. 8A) may reflect a requirement by the small molecule inhibitor to accumulate at sufficient levels in a suitable form (e.g. the fraction of **3f** unbound by other non-PCSK9 plasma proteins) to effect a decrease in total cholesterol. This point is a subject of ongoing studies.

In parallel with the analysis of samples for total cholesterol, plasma samples were also assayed for their levels of PCSK9 protein. Fig. 8B shows that two conditions, namely exposure to evolocumab (10 mg/kg/5 days on day 15) and compound **3f** (16.4 mg/kg/day on day 10), significantly increased the levels of circulating PCSK9 beyond those observed in vehicle-treated controls. An increase in circulating PCSK9 levels may be attributed to drug-induced impairment of PCSK9 uptake by the LDLR of liver cells. More broadly, the results suggest that both evolocumab and compound **3f** are engaging PCSK9 and suppressing its function *in vivo* as intended. It is notable that a similar effect was observed by Zhang *et al.*⁴⁵ who reported a large increase in circulating PCSK9 in the plasma of mice treated with their monoclonal antibody (1B20) against PCSK9. Mice exposed to 10 mg/kg/day 1B20 demonstrated an increase of ~750% in total plasma PCSK9 levels, a result that was ascribed to the sequestration of PCSK9 within plasma by the antibody.⁴⁵ It is highly likely that a similar response was recapitulated in the present study by evolocumab and compound **3f**. Collectively, these results have established a proof-of-concept that the impairment of PCSK9 by a small organic molecule can yield a significant, albeit modest decrease in total plasma cholesterol *in vivo*.

² While it was intended that mice were to be dosed with 4 and 20 mg/kg/day, human error led to the use of 3.28 and 16.4 mg/kg/day instead.

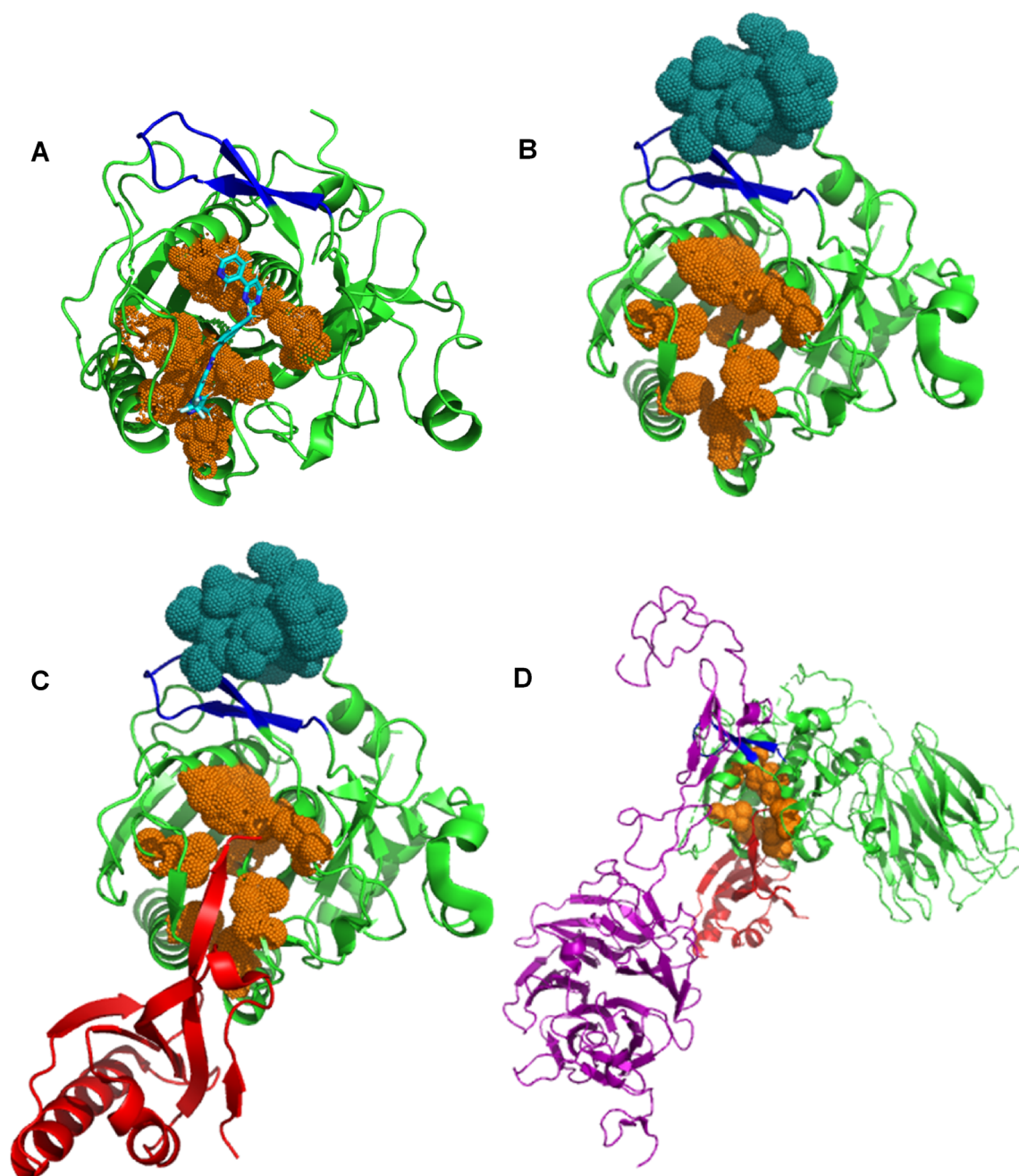


Fig. 9. (A–D) The location of the putative binding site of nilotinib in the context of pre-existing PCSK9 X-ray crystal structures represented as cartoons. The colour scheme from panel (A) has been maintained with the residue side-chains lining the putative nilotinib binding site highlighted in copper orange and emphasised as dotted atomic spheres. (B, C) The locus of the nilotinib binding site as shown in the X-ray crystal structure (PDB code 4NMX).¹⁰ The green PCSK9 catalytic domain is in complex with a peptide inhibitor designated Pep2-8 and shown in dark teal as dotted atomic spheres.¹⁰ The complex is presented in the absence (B) and presence (C) of the prodomain displayed in red. Note that the crystal structure does not include the C-terminal domain of PCSK9. (D) The binding site of nilotinib shown in the context of the PCSK9-LDLR X-ray crystal structure complex as detailed by Lo Surdo *et al.* (²⁸ and PDB code 3P5C). The LDLR is depicted in purple and was crystallised with mature PCSK9 as a truncation of the full-length receptor.²⁸

3.9. The interaction of compound **3f** with PCSK9

Having established proof-of-concept with **3f** *in vivo* (Fig. 8), it is reasonable to briefly speculate on the interaction of the compound with PCSK9 at a molecular level. Fig. 9 provides a direct comparison of the modelled putative binding site (using nilotinib as an exemplar ligand) in the catalytic domain of PCSK9 (Fig. 9A) with existing X-ray crystal structures of the protein including PCSK9 in complex with a peptide inhibitor (Pep2-8) developed by Genentech (Fig. 9B and C, PDB code

4NMX and¹⁰). Pep(2–8) disrupts LDLR binding through a direct interaction with the EGF-A binding region of PCSK9 (Figs. 1A and 3A), a locale that is clearly distinct from the putative binding site of nilotinib (compare Fig. 9A and B). Moreover, a comparison of the binding site in the absence (Fig. 9B) and presence (Fig. 9C) of the prodomain demonstrates a clear overlap in the three-dimensional space occupied by nilotinib and the prodomain, suggesting a source of potential competition for binding to PCSK9. It is currently unclear how compound **3f** and analogues engage the catalytic domain when it is pre-complexed with

its prodomain, as was the case in the binding assay and as circulating PCSK9 *in vivo*.^{1,3} In any case, it is clear that compound **3f** engages PCSK9 to effect disruption of its binding with LDLR (Table 3 and Fig. 9D). X-ray crystallography studies of the **3f**-PCSK9 complex are underway and results will be reported in due course.

3.10. Conclusions

In summary, a small molecule inhibitor of the PCSK9-LDLR interaction has been identified following the discovery that nilotinib modestly disrupted the interaction. A subsequent medicinal chemistry campaign focused on minimising the off-target kinase inhibitory activity of nilotinib, promoting activity in disrupting the PCSK9-LDLR interaction and introducing structural features intended as favourable in the context of pharmacokinetic properties. Compound **3f** emerged from the campaign by demonstrating disruption of the PCSK9-LDLR interaction at nanomolar levels *in vitro* and little inhibitory activity against a small panel of tyrosine kinases. The compound restored LDL uptake by liver cells cultured in the presence of PCSK9 and demonstrated excellent bioavailability when delivered subcutaneously in mice. Most significantly, compound **3f** lowered total cholesterol levels in the plasma of wild-type mice, thereby providing proof-of-concept that the notion of a small molecule inhibitor against PCSK9 is therapeutically viable.

Declaration of Competing Interest

B.J.E., A.K.S., J.P., G.E.K. and J.B. are employees of Nyrada Inc., a subsidiary of Noxopharm Ltd. G.E.K. is the founder and an Executive Chairperson of Noxopharm Ltd., the founder and a Non-Executive Director of Nyrada Inc., and a shareholder of both Noxopharm Ltd. and Nyrada Inc. I.D. is a Non-Executive Director and shareholder of Noxopharm Ltd. and is the owner and Director of Altnia Group, a shareholder of Nyrada Inc. J.T.P. and G.L. are members of the Scientific Advisory Board of Nyrada Inc. B.J.E., J.T.P., G.L., I.D., G.E.K. and J.B. have share/stock options in Nyrada Inc. J.T.P., H.T., J.Z. and I.D. are listed as inventors on the patent that discloses a subset of the compounds described in this manuscript. J.T.P., G.L., B.N., K.C., H.T., J.Z., Q.Z., J.W., Y.T., W.T., Y.X., A.K.R. and S.K. are employees or members of their respective companies or laboratories who were contracted and/or consulted by Nyrada Inc. to perform specific research activities.

Appendix A. Supplementary material

Supplementary data to this article can be found online at <https://doi.org/10.1016/j.bmc.2020.115344>.

References

- Awan Z, Baass A, Genest J. Proprotein convertase subtilisin/kexin type 9 (PCSK9): lessons learned from patients with hypercholesterolemia. *Clin Chem*. 2014;60:1380–1389.
- Lambert G, Sjouke B, Choque B, Kastelein JJ, Hovingh GK. The PCSK9 decade. *J Lipid Res*. 2012;53:2515–2524.
- Horton JD, Cohen JC, Hobbs HH. PCSK9: a convertase that coordinates LDL catabolism. *J Lipid Res*. 2009;50(Suppl):S172–S177.
- Hampton EN, Knuth MW, Li J, Harris JL, Lesley SA, Spraggon G. The self-inhibited structure of full-length PCSK9 at 1.9 Å reveals structural homology with resistin within the C-terminal domain. *Proc Natl Acad Sci U S A*. 2007;104:14604–14609.
- Kwon HJ, Lagace TA, McNutt MC, Horton JD, Deisenhofer J. Molecular basis for LDL receptor recognition by PCSK9. *Proc Natl Acad Sci U S A*. 2008;105:1820–1825.
- Abifadel M, Varret M, Rabes JP, et al. Mutations in PCSK9 cause autosomal dominant hypercholesterolemia. *Nat Genet*. 2003;34:154–156.
- Cohen J, Pertsemlidis A, Kotowski IK, Graham R, Garcia CK, Hobbs HH. Low LDL cholesterol in individuals of African descent resulting from frequent nonsense mutations in PCSK9. *Nat Genet*. 2005;37:161–165.
- Cohen JC, Boerwinkle E, Mosley Jr TH, Hobbs HH. Sequence variations in PCSK9, low LDL, and protection against coronary heart disease. *N Engl J Med*. 2006;354:1264–1272.
- Mullard A. Nine paths to PCSK9 inhibition. *Nat Rev Drug Discov*. 2017;16:299–301.
- Zhang Y, Eigenbrot C, Zhou L, et al. Identification of a small peptide that inhibits

- PCSK9 protein binding to the low density lipoprotein receptor. *J Biol Chem*. 2014;289:942–955.
- Schroeder CI, Swedberg JE, Withka JM, et al. Design and synthesis of truncated EGF-A peptides that restore LDL-R recycling in the presence of PCSK9 *in vitro*. *Chem Biol*. 2014;21:284–294.
- Zhang Y, Ulsch M, Skelton NJ, et al. Discovery of a cryptic peptide-binding site on PCSK9 and design of antagonists. *Nat Struct Mol Biol*. 2017;24:848–856.
- Londregan AT, Wei L, Xiao J, et al. Small molecule proprotein convertase subtilisin/kexin type 9 (PCSK9) inhibitors: Hit to lead optimization of systemic agents. *J Med Chem*. 2018;61:5704–5718.
- Dadu RT, Ballantyne CM. Lipid lowering with PCSK9 inhibitors. *Nat Rev Cardiol*. 2014;11:563–575.
- Sabatine MS, Giugliano RP, Wiviott SD, et al. Open-label study of long-term evaluation against efficacy and safety of evolocumab in reducing lipids and cardiovascular events. *N Engl J Med*. 2015;372:1500–1509.
- Lintner NG, McClure KF, Petersen D, et al. Selective stalling of human translation through small-molecule engagement of the ribosome nascent chain. *PLoS Biol*. 2017;15:e2001882.
- Taechalertpaisarn J, Zhao B, Liang X, Burgess K. Small molecule inhibitors of the PCSK9-LDLR interaction. *J Am Chem Soc*. 2018;140:3242–3249.
- Fitzgerald K, Frank-Kamenetsky M, Shulga-Morskaya S, et al. Effect of an RNA interference drug on the synthesis of proprotein convertase subtilisin/kexin type 9 (PCSK9) and the concentration of serum LDL cholesterol in healthy volunteers: a randomised, single-blind, placebo-controlled, phase 1 trial. *Lancet*. 2014;383:60–68.
- van Poelgeest EP, Hodges MR, Moerland M, Tessier Y, Levin AA, Persson R, Lindholm MW, Dumong Erichsen K, Orum H, Cohen AF, Burggraaf J. Antisense-mediated reduction of proprotein convertase subtilisin/kexin type 9 (PCSK9): a first-in-human randomized, placebo-controlled trial. *Br J Clin Pharmacol*. 2015;80:1350–1361.
- Ding Q, Strong A, Patel KM, et al. Permanent alteration of PCSK9 with *in vivo* CRISPR-Cas9 genome editing. *Circ Res*. 2014;115:488–492.
- Wang X, Raghavan A, Chen T, et al. CRISPR-Cas9 targeting of PCSK9 in human hepatocytes *in vivo*-brief report. *Arterioscler Thromb Vasc Biol*. 2016;36:783–786.
- Petersen DN, Hawkins J, Ruangsiriluk W, et al. A small-molecule anti-secretagogue of PCSK9 targets the 80S ribosome to inhibit PCSK9 protein translation. *Cell Chem Biol*. 2016;23:1362–1371.
- McClure KF, Piotrowski DW, Petersen D, et al. Liver-targeted small-molecule inhibitors of proprotein convertase subtilisin/kexin type 9 synthesis. *Angew Chem Int Ed Engl*. 2017;56:16218–16222.
- Xu S, Luo S, Zhu Z, Xu J. Small molecules as inhibitors of PCSK9: Current status and future challenges. *Eur J Med Chem*. 2019;162:212–233.
- Min DK, Lee HS, Lee N, et al. *In silico* screening of chemical libraries to develop inhibitors that hamper the interaction of PCSK9 with the LDL receptor. *Yonsei Med J*. 2015;56:1251–1257.
- Gilson MK, Liu T, Baitaluk M, et al. A public database for medicinal chemistry, computational chemistry and systems pharmacology. *Nucl Acids Res*. 2015;44(2016):D1045–D1053.
- MedChemSoft, Solutions. *Modeling kinase inhibition: Our predictions vs crystal structure*. 2016 (accessed July 09, 2019).
- Lo Surdo P, Bottomley MJ, Calzetta A, et al. Mechanistic implications for LDL receptor degradation from the PCSK9/LDLR structure at neutral pH. *EMBO Rep*. 2011;12:1300–1305.
- Berman HM, Westbrook J, Feng Z, et al. The Protein Data Bank. *Nucl Acids Res*. 2000;28:235–242.
- Kee AJ, Chagan J, Chan JY, et al. On-target action of anti-tropomyosin drugs regulates glucose metabolism. *Sci Rep*. 2018;8:4604.
- Manley PW, Druceckes P, Fendrich G, et al. Extended kinase profile and properties of the protein kinase inhibitor nilotinib. *Biochim Biophys Acta*. 1804;2010:445–453.
- Cai H, Smith DA, Memarzadeh S, Lowell CA, Cooper JA, Witte ON. Differential transformation capacity of Src family kinases during the initiation of prostate cancer. *Proc Natl Acad Sci U S A*. 2011;108:6579–6584.
- Xing L, Rai B, Lunney EA. Scaffold mining of kinase hinge binders in crystal structure database. *J Comput Aided Mol Des*. 2014;28:13–23.
- Fala L. Repatha (Evolocumab): second PCSK9 inhibitor approved by the FDA for patients with familial hypercholesterolemia. *Am Health Drug Benefits*. 2016;9:136–139.
- Gibbs JP, Doshi S, Kuchimanchi M, et al. Impact of target-mediated elimination on the dose and regimen of evolocumab, a human monoclonal antibody against proprotein convertase subtilisin/kexin type 9 (PCSK9). *J Clin Pharmacol*. 2017;57:616–626.
- Abdel-Meguid SS, Elshourbagy N, Meyers H, Mousa SA. (WO2014150326) *Anti-protein convertase subtilisin kexin type 9 (Anti-PCSK9) compounds and methods of using the same in the treatment and/or prevention of cardiovascular diseases*. 2014.
- Cunningham D, Danley DE, Geoghegan KF, et al. Structural and biophysical studies of PCSK9 and its mutants linked to familial hypercholesterolemia. *Nat Struct Mol Biol*. 2007;14:413–419.
- Fisher TS, Lo Surdo P, Pandit S, et al. Effects of pH and low density lipoprotein (LDL) on PCSK9-dependent LDL receptor regulation. *J Biol Chem*. 2007;282:20502–20512.
- Theirez A, Blom DJ, Ramin-Mangata S, et al. Homozygous familial hypercholesterolemia patients with identical mutations variably express the LDLR (low-density lipoprotein receptor): implications for the efficacy of evolocumab. *Arterioscler Thromb Vasc Biol*. 2018;38:592–598.
- Schwartz GG, Steg PG, Szarek M, et al. Investigators, alirocumab and cardiovascular outcomes after acute coronary syndrome. *N Engl J Med*. 2018;379:2097–2107.
- Wang X, Paigen B. Genetics of variation in HDL cholesterol in humans and mice. *Circ Res*. 2005;96:27–42.
- Yin W, Carballo-Jane E, McLaren DG, et al. Plasma lipid profiling across species for

- the identification of optimal animal models of human dyslipidemia. *J Lipid Res.* 2012;53:51–65.
43. Marais AD. Apolipoprotein E in lipoprotein metabolism, health and cardiovascular disease. *Pathology.* 2019;51:165–176.
44. Zaid A, Roubtsova A, Essalmani R, et al. Proprotein convertase subtilisin/kexin type 9 (PCSK9): hepatocyte-specific low-density lipoprotein receptor degradation and critical role in mouse liver regeneration. *Hepatology.* 2008;48:646–654.
45. Zhang L, McCabe T, Condra JH, et al. An anti-PCSK9 antibody reduces LDL-cholesterol on top of a statin and suppresses hepatocyte SREBP-regulated genes. *Int J Biol Sci.* 2012;8:310–327.